2014

Using Acoustic Emission Monitoring for Energy-based Fatigue Life Prediction

Sepehr Nesaei
South Dakota State University

USING ACOUSTIC EMISSION MONITORING FOR ENERGY-BASED FATIGUE LIFE PREDICTION

BY

SEPEHR NESAEI

A thesis submitted in partial fulfillment of the requirements for the

Master of Science

Major in Mechanical Engineering

South Dakota State University

2014

USING ACOUSTIC EMISSION MONITORING FOR ENERGY-BASED FATIGUE LIFE PREDICTION

This thesis is approved as a creditable and independent investigation by a candidate for the Master of Science in Mechanical Engineering degree and is acceptable for meeting the thesis requirements for this degree. Acceptance of this does not imply that the conclusions reached by the candidates are necessarily the conclusions of the major department.

Dr. Fereidoon Delfanian, Ph.D.
Major Advisor Date

Dr. Todd Letcher, Ph.D.
Thesis Advisor Date

Dr. Kurt Bassett, Ph.D.
Head, Department of Mechanical Engineering Date

Dean, Graduate School Date

Dedicated to my late mother (Sara)

ACKNOWLEDGEMENTS

This research was supported by the Material Evaluation and Testing Laboratory (METLAB) in the Mechanical Engineering Department at the South Dakota State University and was accomplished under the supervision of Professor Fereidoon Delfanian.

Foremost, I would like to express my sincere gratitude to my major advisor Dr. Fereidoon Delfanian for his continuous support of my graduate study, research and employment. My special thanks go to my thesis advisor Dr. Todd Letcher whose encouragement during my research and his continuous supports and knowledge. He guided and assisted me from the beginning to the completion of this project. My many thanks go to Dr. Sepand Momeni from Physical Acoustic Corporation (PAC) who helped and guided me during this research. His valuable practical experience to conduct the experiments is appreciated.

My special thanks will also go to my dearest family members, my father and my kind sisters whose guidance and supports were always with me through my life and career. My life and academic successes are due to my late beloved mother's love, encouragements and supports. I miss her a lot.

Finally, I would like to dedicate this thesis to my lovely wife, Samaneh whose encouragements, supports and patience have given me the strengths to complete my M.S study. I am really lucky and grateful to have her in my life.

CONTENTS

LIST OF FIGURES

LIST OF TABLES

ABSTRACT

USING ACOUSTIC EMISSION MONITORING FOR ENERGY-BASED FATIGUE LIFE PREDICTION

SEPEHR NESAEI

2014

The study of fatigue and fracture mechanics is crucial to the health monitoring and overall safety of aerospace and civil structures. The materials used to manufacture these industry parts have inherent anomalies that eventually grow under cyclic loadings during regular operation. The ASTM and/or military testing guidelines used to analyze and qualify structures and materials for use are costly and time consuming. Therefore, any additional methods or knowledge that can be used to reduce the number of tests will be useful to the industry to avoid unnecessary costs. Acoustic emission (AE) monitoring is currently used in many applications to assess the structural health and remaining useful life in various civil and mechanical applications. Its capability to assess smaller crack growth well before any strain monitoring system can help for early structural lifetime estimation.

The main goal of this thesis was to develop a method using acoustic emission monitoring for fatigue life predictions similar to a strain energy-based fatigue life prediction method. Experiments were conducted to determine acoustic energy parameters and patterns at various stress levels during constant stress fatigue testing. This information was used to make life predictions which were then compared to experimentally obtained data. Statistical evaluation of the correlation assured the dependencies between the energy variables.

Hysteresis energy and acoustic energy methods were applied to the experimental data. Both methods provide good estimations of fatigue life, however, the acoustic energy method show 15% to 23% better results depending on specimen design and material.

1 INTRODUCTION

1.1 Motivation

Recent failures of several major structures, such as pressure vessels, storage tanks, ships, aircrafts, gas pipe lines, bridges, dams, and other welded parts such as those shown in Figure 1.1 have brought the issue of health monitoring and maintenance of critical structures to the general public's attention. Concerns about issues like loss of life, environmental safety, and high costs associated with repair and replacement of components which have been estimated to be in the millions of dollars have become critically important. In almost all cases, these failures occurred during structural usage where cracks have initiated and advanced in a stable manner to failure under the fatigue loads well below the material's allowable yield point [1].

Figure 1.1 Mianus River Bridge Collapse [2] & Boeing 737 Fuselage Failure[3]

In-depth scientific investigation into the nature of these failures indicated that several factors (shown below) can contribute to an accelerated crack growth, resulting in catastrophic failure, and in some cases, loss of Lives [1]:

- Poor structural design practices (e.g., stress concentrations, insufficient material ductility, etc.)
- Residual stresses remaining from fabrication and manufacturing
- Lack of adequate NDI(Non- Destructive Inspection) inspections
- Material degradation in harsh environments (e.g., high/low-temperatures, corrosive environments, etc.)

Typically, a process as shown in Figure 1.2 is implemented to study crack growth/residual strength analysis with an emphasis on the comparison (feedback) of analyses [1]. Each step of the analysis requires both fatigue and fracture mechanics knowledge of the material. It requires performing several experimental tests according to related ASTM standards which are typically costly, and labor/time consuming. Finding alternative techniques which can reduce the amount of time and cost are always beneficial.

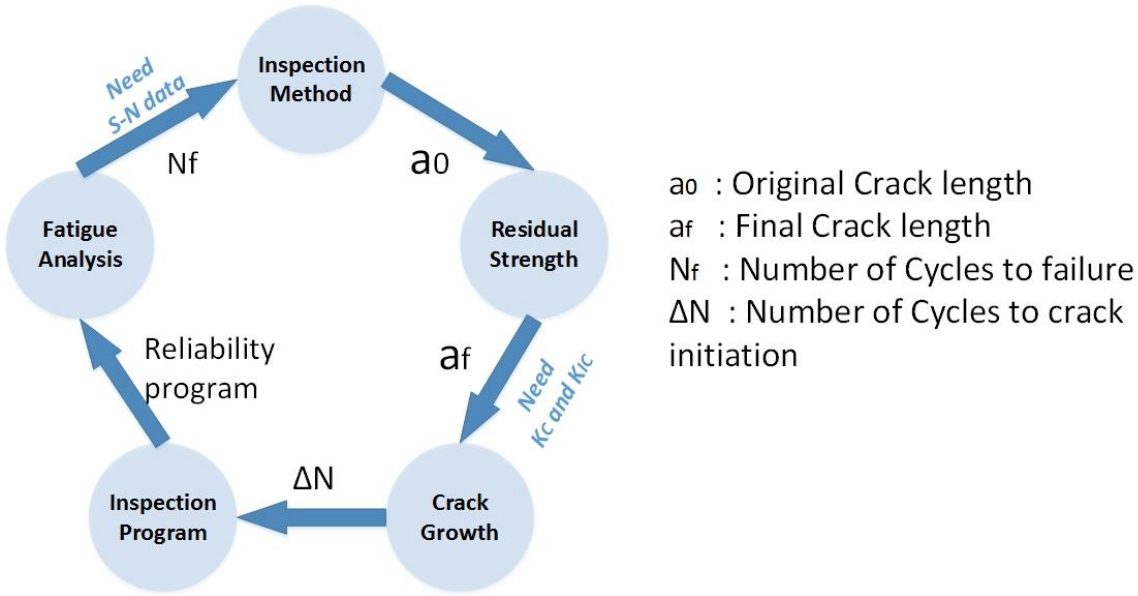

Figure 1.2 Feedback analyses to determine structural safety

1.2 Literature Review

Most fatigue life prediction methods, such as full S-N (Stress- Number of cycles to failure) curves, require large amounts of empirical data. This empirical data requires a significant amount of testing time on expensive equipment. It would extremely beneficial to be able to develop a method that reduces the amount of empirical data required to make fatigue predictions. This led to the development of an energy-based fatigue life prediction method [4]. The main idea behind this method states that the total monotonic energy divided by the cyclic hysteresis energy provides an estimate for the lifetime of a specimen at different load ranges. This method has shown to be effective in several studies by testing unnotched dog-bone shaped specimens using Al6061-T6 and Ti64. The estimations were plotted in a typical S-N curve and compared with the experimental results to show the accuracy and applicability of this method [5][6][7][8][9].

Scott-Emuakpor et al. applied the strain energy method to aluminum alloys both for multi-axial and shear loadings [8]. Experimental results for both fatigue methods were compared for aluminum alloy samples. This research supports the entire energy-based fatigue life prediction criterion [8]. The framework of their paper is an extension of previous research analyzing a uni-axial energy based-fatigue life prediction method. Before that, they analyzed all material properties related to monotonic strain energy. Then, the variation of monotonic strain energy density as the physical damage quantity was assessed by three sigma probabilistic results. By incorporating the sigma results into the proposed fatigue life energy method, the accuracy of life for Ti64 could be improved [4].

Recently, Letcher et al. modified the energy based fatigue life predication method. The new approach was followed by running short term fatigue testing at different stress levels on a round dog bone shaped aluminum specimen. Results were then plotted in a stress versus strain curve using the failure/energy correlation. The new fatigue life assessment method suggested a new way to explore the appropriateness of the prediction method [10]. More experiments should be conducted on other material types and also on notched flat specimens by applying either the strain energy method or the modified version of it. Conducting more tests at different load ratios helps to certify the appropriateness and applicability of the proposed method.

On the other hand, geometric and environment effects such as notch size and temperature change in fatigue lifetime of specimens has also been investigated. Fatemi investigated both notch severity effect and notch constraint condition on fatigue behavior of micro alloyed (MAF) forging steel and the quenched and tempered (QT) steels [11]. Corresponding experimental results in the form of S-N curve and strain life approaches were evaluated. Finally, notched fatigue behavior between these two types of specimens was compared. Based on the experimental result analysis round specimens have about the same notch fatigue strength under plain strain conditions for both types. Plate specimens have also the same notch fatigue strength at shorter lives for both types, but MAF grade has lower values at longer lives [11].

Several studies were done by employing the common fracture mechanics parameters such as the stress intensity factor (K), the J-integral, the Crack- Tip Opening Displacement (CTOD) and the Crack- Tip Opening Angle (CTOA) to predict the fatigue lifetime of the specimens [12]. In the majority of studies, the crack growth rate is used as

a key parameter for estimation purposes. In several studies, the acoustic emission technique was used as a nondestructive technique to monitor the fatigue and fracture behavior of materials. For example, Carlyle et al used the fatigue analyzer apparatus to capture the acoustic emission events by defining three series of experiments and comparing the results with traditional AE monitoring systems [13]. They included the detection of fatigue crack propagation at less than maximum load during spectrum loading of Monel 400, the quick change in load dependence of an active AE source in graphite/epoxy, and the existence of crack closure at high tensile stress levels during falling load in 300M steel. [13].

Later, Roberts et al. investigated the correlation between crack growth rates and acoustic emission counts by using filtered acoustic data for different percentages of the fatigue load range from the peak load [14]. To do this, AE monitoring during the fatigue cyclic tests was conducted on steel and welded steel compact tension specimens and T-section girders [14]. Results indicated the benefits of using short term AE monitoring to predict the fatigue lifetime of the damaged structures. Kohn et al. used Ti-6Al-4V specimens to detect and locate crack extensions of approximately 10 μm in a cyclic testing [15]. AE techniques were used as a warning of material failure. According to their research, three distinct stages in the failure process emerged during fatigue loading. The stages are crack initiation, slow crack propagation and rapid crack propagation. The stages are differentiated by the rate of acoustic emission event accumulation [15]. The main problems related to incorporating crack growth and propagation into the fatigue life prediction methodology are the burden of time, cost, and labor in the testing methods according to ASTM standards.

Other studies were done by using the acoustic emission technique combined with pattern recognition algorithms to estimate the fatigue lifetime of specimens without using any information regarding the crack growth rate. Barsoum et al. used AE nondestructive methodology to monitor the fatigue crack growth behavior in axially loaded notched specimens made of structural steel [16]. Kohonen self-organizing map (SOM) artificial network was implemented to identify the failure modes of plastic deformation including plane stress and plane strain fracture. Later, back propagation neural network (BPNN) was used to perform fatigue life prediction, first based on the first quarter (0-25%) of the experimental life cycle and then on the third quarter (50-75%) of fatigue life data. The results were then compared with the damage tolerance analysis software Air Force Growth (AFGROW) for the linear elastic fracture mechanics (LEFM) [16]. The problem with using the supervised classifiers such as neural networks along with experimental data points is the necessity of having enough training data sets in order to have more accurate prediction results. In addition, the scattering nature of the acoustic signals is accompanied by background and instrumentation noise which make it more difficult to be used in such estimation techniques.

1.3 Objective

The purpose of this thesis is to investigate relationship between acoustic emission energy and hysteresis energy by applying the modified energy-based fatigue life prediction framework to the acoustic emission monitoring methodology.

The following procedures will be implemented:

- Investigate the link between AE energy parameters and fatigue life estimation
- Conduct experiments to determine acoustic emissions energy values at various stress levels for constant stress fatigue testing
- Use this information in conjunction with current strain monitoring techniques to provide life estimation and better health monitoring of in-use structures
- Investigate the geometry change and notch size effect of the specimens in the fatigue lifetime framework

2 THEORETICAL METHOD

2.1 Acoustic Emission and Life Prediction

Acoustic emission (AE) testing is a passive non-destructive inspection techniques [17]. As it is depicted in Figure 2.1, crack growth inside the material due to a stress concentrator acts as an acoustic emission source. Appropriate instrumentation must be used to detect the acoustic emissions and turn these emissions in to electrical signals. This instrument consists of sensors, preamplifiers and data acquisition and signal processing units.

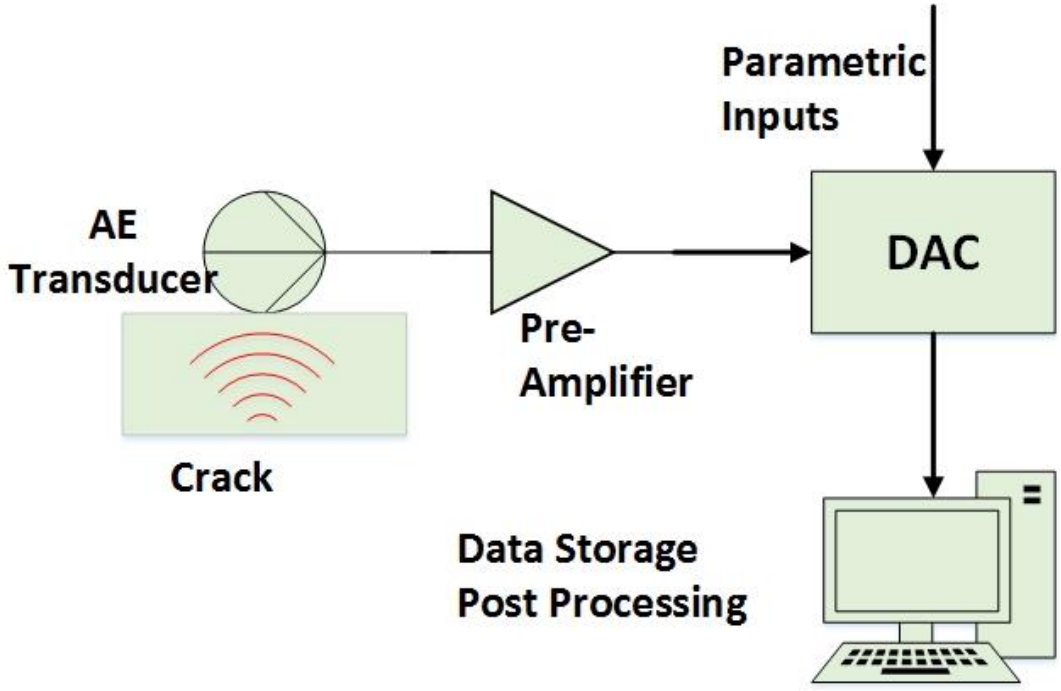

Figure 2.1 Schematic of a typical AE monitoring system setup

Typically, two types of elastic waves or modes exist in wave propagation theory. The compression or primary (p-) wave is where the direction of the particles is parallel to the direction of the wave. The second type is the shear or the (s-) wave where the

direction of the particles' movement is perpendicular to the direction of wave propagation [18].

The p-wave velocity in an isotropic, homogeneous and elastic body can be calculated from E, ρ and ϑ as in Equation 2.1:

$$C_p = \sqrt{\frac{E}{\rho}}\sqrt{\frac{1-\nu}{(1+\nu)(1-2\nu)}} \qquad \text{Equation 2.1}$$

where E is the dynamic Modulus of Elasticity in N/m^2, ρ the material density in kg/m^3, and ϑ Poisson's Ratio. In addition, there is a third type of wave named surface or Rayleigh (R-) which has $C_p > C_s > C_R$ relationship with the two others [18].

AE signals are captured by piezo-electric sensors mounted on the surface of the specimens. The sensors are sensitive to frequencies change from approximately 10 to 500 KHz. The analogue signals captured are amplified and digitized to be stored by a computer [17] .

A typical AE waveform is shown in Figure 2.2. Various factors contribute to the shape of the waveform. The waveform shape depends on a) The characteristics of the AE source event b) wave propagation behavior (e.g. wave modes, wave velocity, attenuation, reflection and signal interference) c) AE sensor response. Sensor and material responses can cause the received signals to be distorted and can cause the recorded signals to be considerably different from the original pulses [19].

Amplitude, A, as can be seen in Figure 2.2, is the largest measured voltage in dB unit in a signal. Also Threshold is the user-defined value that only recorded signals in an emission above this value are accepted.

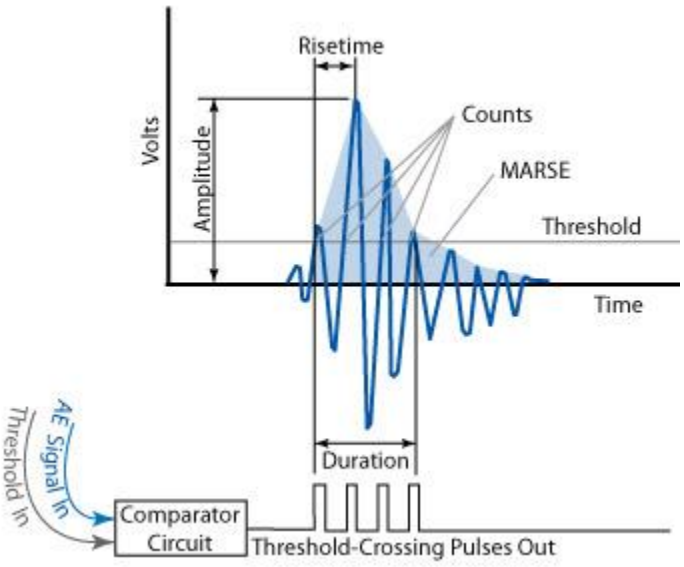

Figure 2.2 Important features of an AE hit [19]

MARSE (Measured Area under the Rectified Signal Envelope), E or U, known as energy counts is the measured area under the envelope of a corrected linear voltage-time curve obtained from a transducer. This AE feature is affected by the other features such as duration and amplitude of the signal. It should be noted that acoustic emission "energy" is the main focus of this study. Other AE characteristics as defined in the Figure 2.2 are Rise time, R, Duration, D and Counts, n [19].

The relationship between the fatigue crack growths with AE have been used in structural damage evaluation [20]. Commonly used parameters in Linear Elastic Fracture

Mechanics (LEFM) include crack length, crack growth rate, da/dN and stress intensity factor, ΔK that are used in fatigue damage detection and life prediction [20].

A representative fatigue crack growth rate curve is shown in Figure 2.3. AE monitoring of a specimen under cyclic loading can demonstrate 3 distinct regions. The threshold and accelerated regions (first and third regions) are dependent on stress ratio, R and the microstructural behavior of the material. But the secondary region, Paris-Erdogan region, is stable [20][21][22].

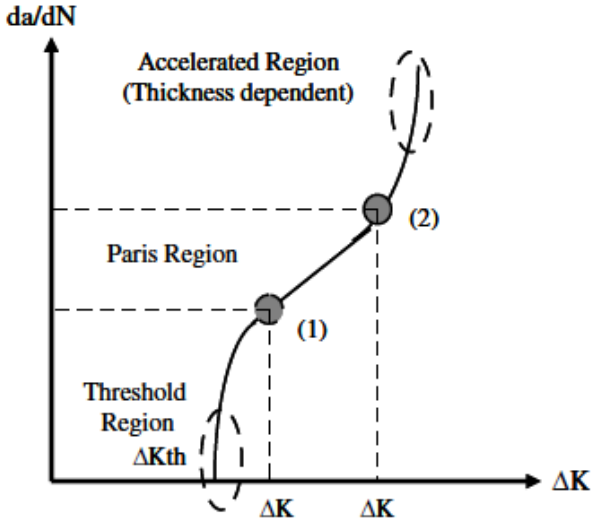

Figure 2.3 A schematic of fatigue crack growth rate curve [22]

In previous studies, count rate of AE signals was used to establish a relationship between the AE signals and crack growth behavior [23]. Their model was based on the relationship between the AE count rate, dn/dN and stress intensity factor, ΔK by connecting the crack released energy to AE counts[23].

The measured acoustic emission outputs consist of three energy features: 1) AE energy 2) Signal strength and 3) Absolute energy. AE energy and Signal strength represent the area under the corrected signal envelope; though the former has higher resolution. Absolute energy is obtained from the integration of the squared voltage signal divided by a reference resistance over the duration of an acoustic emission.

According to Figure 2.3, the stable crack growth region (Stage II) in a material, can be formulized by Paris Law (Equation 2.2) [24].

$$\frac{da}{dN} = C(\Delta K)^m \qquad \text{Equation 2.2}$$

where C and m are material constants. Assuming that the absolute energy of an AE signal, U, is proportional to crack released energy $\left[\frac{\Delta K^2}{(E'.(1-R)^2)}.t.a\right]$, a relationship between the AE absolute energy rate and stress intensity range is obtained by Equation 2.3[20].

$$\frac{dU}{dN} = B_e(\Delta K)^p \qquad \text{Equation 2.3}$$

where $B_e = \frac{BtC}{(E'(1-R)^2)}$ and p$= m + 2$. E' is equal to E (modulus of elasticity) for plane stress case and E/(1-ν^2) for plane strain case. Traditionally, all fatigue crack growth constants (c, n, K_C, and ΔK_{th}), shown in Equation 2.2 and Figure 2.3, will be provided through experimental testing, which is costly, labor intense and time consuming.

Later, accumulated and cyclic acoustic emission energy values will be used to make fatigue life predictions at various stress levels – similar to a method that uses hysteresis strain energy to predict fatigue life of a specimen of material.

2.2 Strain Energy Method and Life Prediction

A method for quickly estimating an S-N curve for a material has recently been developed. The main theory behind this idea states that fatigue life can be estimated by dividing the total monotonic energy by the cyclic strain energy at any given stress level [6]. The primary energy based fatigue theory was tested using round dog-bone shaped specimens axially, torsionally and at elevated temperatures.

First, a model was created for the behavior of the true stress/strain curve from a monotonic test as shown in Equation 2.4 where the term σ_0 was defined by Equation 2.5 [6].

$$\varepsilon = \frac{\sigma}{E} + \varepsilon_0 \sinh\left(\frac{\sigma}{\sigma_0}\right) \qquad \text{Equation 2.4}$$

$$\sigma_0 = \frac{\sigma_f - \sigma_y}{\ln(\frac{\varepsilon_n}{0.002})} \qquad \text{Equation 2.5}$$

where f subscript indicates final fracture while y subscript indicates yield. Next, a model was developed for the stress/strain relationship for a hysteresis loop (Figure 2.4) in a fatigue cycle. This model is shown in Equation 2.6. The model was created using a generalized coordinate system as depicted in Figure 2.4 [25].

$$\varepsilon_{pp} = \frac{\sigma_{pp}}{E} + \frac{1}{C}\sinh\left(\frac{\sigma_{pp}}{\sigma_C}\right) \qquad \text{Equation 2.6}$$

where $_{pp}$ subscript means peak to peak in the generalized coordinate system. The coefficients "C" and "σ_C" are the adjusted scalar coefficients used to model the hysteresis loop size and shape.

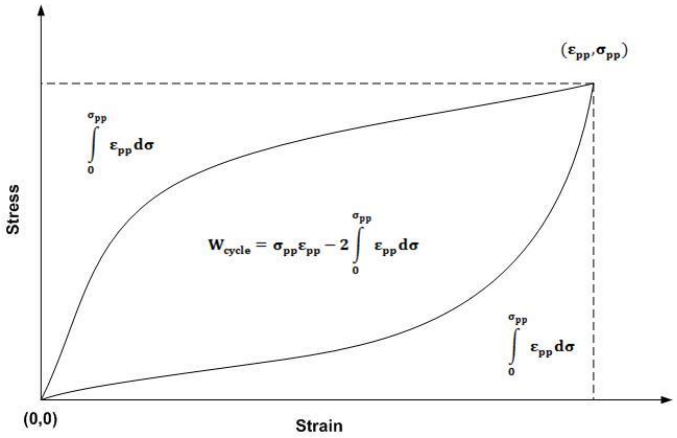

Figure 2.4 Hysteresis loop in generalized coordinates [5]

The strain energy for a single fatigue cycle is obtained as depicted in Figure 2.4. The integral inside the hysteresis loop can be calculated by assuming that the loop is symmetric about a line from origin (0,0) to the maximum stress-strain point (ε_{pp},σ_{pp}) as shown in Equation 2.7. Equation 2.8 shows the resulting equation when $2\sigma_a$ is substituted for σ_{pp} and the integral is evaluated.

The material toughness, or the total strain energy accumulated in a monotonic test divided by the strain energy accumulated in one hysteresis loop can then be used to determine the expected lifetime of a specimen using Equation 2.9[5].

$$W_{cycle} = \sigma_{pp}\varepsilon_{pp} - 2\int_0^{\sigma_{pp}} \varepsilon_{pp} d\sigma \qquad \text{Equation 2.7}$$

$$W_{cycle} = \frac{2\sigma_C}{C}\left[\frac{\sigma_a}{\sigma_C}\sinh\left(\frac{2\sigma_a}{\sigma_C}\right) - \cosh\left(\frac{2\sigma_a}{\sigma_C}\right) + 1\right] \qquad \text{Equation 2.8}$$

$$N_f = \frac{\sigma_n\left(\varepsilon_n - \frac{\sigma_n}{2E}\right) - \varepsilon_0\sigma_0\left[\cosh\frac{\sigma_n}{\sigma_0} - 1\right] + \frac{\beta_1}{2}\left(\varepsilon_f^2 - \varepsilon_n^2\right) + \beta_0(\varepsilon_f - \varepsilon_n)}{\frac{2\sigma_c}{C}\left\{\frac{\sigma_a}{\sigma_c}\sinh\left(\frac{2\sigma_a}{\sigma_c}\right) - \left[\cosh\left(\frac{2\sigma_a}{\sigma_c}\right) - 1\right]\right\}} \quad \text{Equation 2.9}$$

2.3 Modified Life prediction methodology

Continuing the recent research on an accelerated fatigue life behavior assessment methods [10], a modified energy based fatigue theory is introduced. Based on this theory, the total number of cycles to failure is proportional to the ratio between the Accumulated Hysteresis Energy (ACHE) over Steady State Hysteresis Energy (SSHE) in a cyclic test. This ratio can be then made into an equation by using α factor (Equation 2.10 and Equation 2.11).

$$N_{predicted} \propto \frac{Ac.Hyst\ Energy}{Steady\ state\ Hyst\ Energy} \quad \text{Equation 2.10}$$

$$N_{predicted} = \alpha\frac{ACHE}{SSHE} \quad \text{Equation 2.11}$$

This new model is used as the main theory for the whole of this study. The new approach is then applied to both hysteresis energy and acoustic emission energy values obtained from the experiments on single edged notched specimens. In order to apply the proposed method to the acoustic emission technique, the elementary step is to find a correlation between the Hysteresis Energy with the acoustic emission energy and the rest of the procedure is similar to the hysteresis part. To do this, the nonlinear correlation between these two quantities was investigated by using Spearman's rank correlation coefficient or Spearman's rho. This coefficient named after Charles Spearman and labeled as ρ is used as a nonparametric measurement tool to show the statistical dependence of

two variables. For a sample of size n, the n number of raw values X_i and Y_i can be converted to ranks x_i and y_i by using the Equation 2.12 [26].

$$\rho = 1 - \frac{6\sum d_i^2}{n(n^2-1)} \qquad \text{Equation 2.12}$$

where $d_i = x_i - y_i$ as the difference between ranks.

3 EXPERIMENTAL METHODS

In this chapter, the experimental procedures to collect necessary data will be introduced. Detailed information will be provided to collect both strain hysteresis loops and acoustic emissions signals.

3.1 Sample Preparation and Test setup

A modified version of the single edge notch specimens, SE(T), were designed based on ASTM E647-08 standard [27]. The effective variable parameters considered in this research to be investigated are listed below:

- Material type - two aluminum alloys (6061-T6 (Style A and Style B) and 7075-T6) were selected based on their ease of availability and application especially in aerospace industries
- Notch size effect- two different notch sizes (45 degree and 60 degree) were used
- Geometry change- two different widths were used to accommodate different crack dimensions
- Grip clearance - two different grip clearance lengths were used

The Figure 3.1 and Figure 3.2 show primary and secondary specimen designs with grip clearance, acoustic sensors mounting positions and dimensions.

All specimens for each alloy were cut by EDM machining from a single plate of material.

Standard procedures to set up the acoustic emission instrumentation following ASTM standard E650/E650M [28] and ASTM E976-10 [29] were used.

Two acoustic sensors were mounted according to Figure 3.1 in the regions specified, one sensor close to the notch and the other closer to the grip area (Figure 3.3). Clay was used to damp vibrations and other noise from the hydraulic grips while held in the MTS machine by the wedge grips.

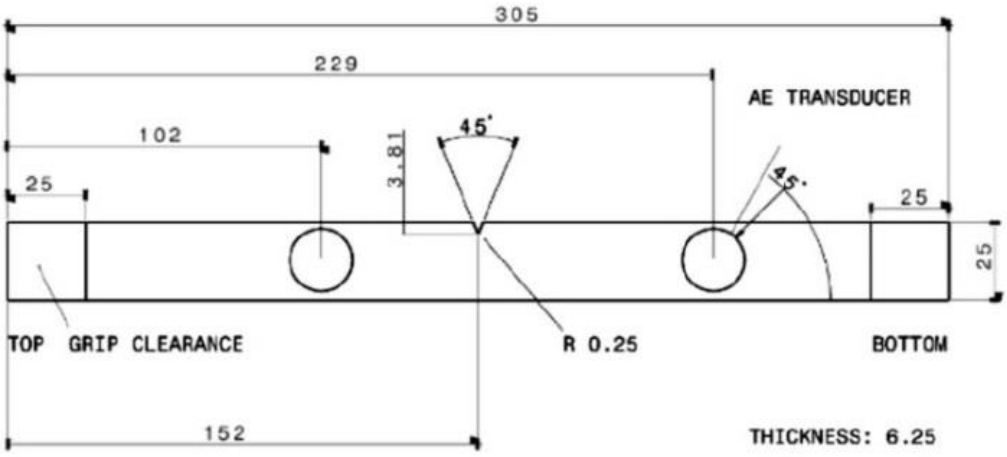

Figure 3.1 Primary specimen design in mm (Aluminum 7075-T6)

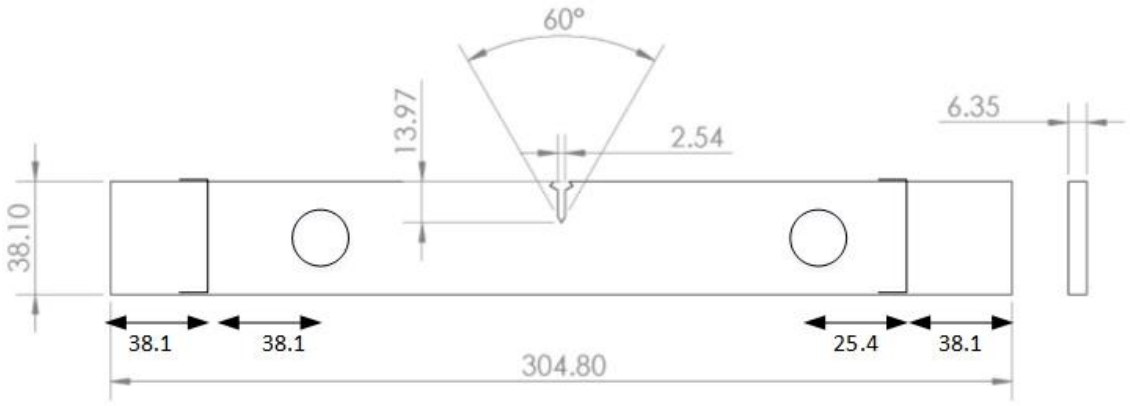

Figure 3.2 Secondary specimen design in mm (Aluminum 6061-T6)

Figure 3.3 Specimen design setups in the MTS machine with acoustic sensors attached and extensometer

A major difficulty in AE fatigue testing is separating the useful AE signal from the noise signal obtained by the testing machine. Choosing the appropriate AE sensors is one of the important steps in order to get better monitoring of the crack growth and propagation. The differences between AE sensors are based on the size, shape, application, frequency and temperature ranges. Experimental procedures were modified and refined throughout the testing. Testing on Al 7075-T6 used Play-doh and Physical Acoustic Corporation (PAC) R15 sensors. Later on the AL 6061-T6 testing, the Play-doh was replaced with modelling clay and the R15 AE sensors with up to 150 KHZ frequency range were replaced with Nano band pass sensors with 200- 400 KHZ frequency ranges. Both changes were made to isolate the actual AE signals and minimize the noise collected by the AE sensors. The 40 dB gain amplifiers were used to amplify the captured signals coming from the sensors.

Also, the 634.31F/24 axial-multiple gage length model of extensometer with 20 mm gage length was used to record strain values throughout the test.

3.2 Fatigue Testing

Fatigue loading was applied by a MTS landmark 370 tensile tester, equipped with 100 KN (22 Kip) load capacity cell. Time, force, machine displacement and strain values for each test were captured at a rate of 200 points per fatigue cycle. Each specimen was fatigued at 2 Hz with load ratio of R=0(Min Load/ Max Load). Testing was conducted at five different stress levels (except for Al7075-T6), which are summarized in Table 3.1. MTS data points were recorded every 2 milliseconds.

Table 3.1 Summary of load ranges

Material Type	Maximum Load Range with R=0
Al 7075- T6	3000 lbs. - 3500 lbs. – 4000 lbs. - 4500 lbs.
Al 6061- T6 - Style A	2500 lbs. - 3000 lbs. – 3500 lbs. – 4000 lbs. - 4500 lbs.
Al 6061- T6 - Style B	2500 lbs. - 2750 lbs. –3000 lbs. – 3250 lbs. - 3500 lbs.

3.3 Acoustic emission testing

The acoustic emission signals were collected using a 4-complete channel digital acoustic emission data acquisition on a single board, PCI/DSP-4 supplied by Physical Acoustic Corporation (MISTRAS). The AE monitoring system consists of three main pieces, AE sensors and amplifiers to capture and amplify the AE signals, data acquisition module to record the data and do the filtration, the AEwin software to visualize and analysis the recorded data. The equipment and software was used to record AE signals which will be analyzed later. As an essential requirement in monitoring a sensor, using enough coupling

between the AE sensors and the surface of the samples is needed. As depicted in the Figure 3.3, Silicon grease and electric tapes were used to increase the acoustic coupling.

The maximum value of the duration was chosen as 100 milliseconds to ensure that all duration signals were captured. The remaining parameters of peak definition time (PDT), hit definition time (HDT) and the hit lock-out time (HLT) as waveform parameters are important to help to separate noise from fatigue data points. The proper setting of the PDT ensures the correct selection of signal peak for rise time measurements. The HDT parameter ensures that a signal hit is picked as only one hit. Choosing the appropriate value of HDT certifies the end of a signal hit. HLT parameter finalizes the measurement process of the hit waveform and stores all of the quantified parameters (amplitude, counts, duration, rise time and energy) in the data acquisition buffer. Insufficient time settings of the HDT and HLT parameters will lead to multiple hit data, where two acoustic emission hits merge and become one hit. This prevents the first hit to be fully stored and finalized before the second hit starts and is recorded [16].

Table 3.2 AE Hardware Settings

Parameter	Value
Pre amplifier	40 dB
Peak Definition Time (PDT)	400 µsec
Hit Definition Time (HDT)	800 µsec
Hit Lock Time (HLT)	5000 µsec
Threshold	40, 45, 50 dB
Sampling rate	2 MSPS
Pre trigger length	256 µsec
Hit length	2K
Analogue filter (band pass)	200- 400 KHZ

The HLT and HDT values are chosen as 800 μsec and 5 milliseconds experimentally and in accordance to pencil break test from different locations of the specimens. The important settings of the AE parameters are listed in Table 3.2.

3.4 Experimental procedure

The first step of the experimental procedure is Threshold determination. As described in ASTM E650-97 [28], the pencil lead break test was performed before running each experiment. Breaking pencil lead simulates an acoustic emission event using the fracture of pencil tip on the surface of the specimens – which can be simulated anywhere on the specimen. This test also helps to set the wave velocity as an AE input parameter. Although source location is not considered as the major outputs of this research, but an average velocity of 170000 in/sec was set as the wave velocity for the linear source location setup. This test was done in accordance to pencil break test. Knowing the fact that the major elastic waves that are produced are guided waves, this velocity seems to be reasonable.

A simple test was used to determine the threshold level for this particular test setup. A silent mode test was conducted with a sample held by the grips and the MTS machine hydraulic pump power was on but fatigue was not applied. AE signals are captured and monitored simultaneously by the AEwin software for 15 minutes to ensure that there was no hit caused by vibrations from the MTS machine. If there were no hits detected from machine vibrations, the threshold level was lowered and checked again. This process continued until the lowest possible threshold value was determined that did not collect hits from vibrations.

During fatigue testing, the AEwin software recorded the acoustic emission signals that crossed this noise threshold level along with load values sent to the AE DAQ by the MTS machine. The fatigue test would continue until the failure with all hits recorded. The entire process is depicted by Figure 3.4 .

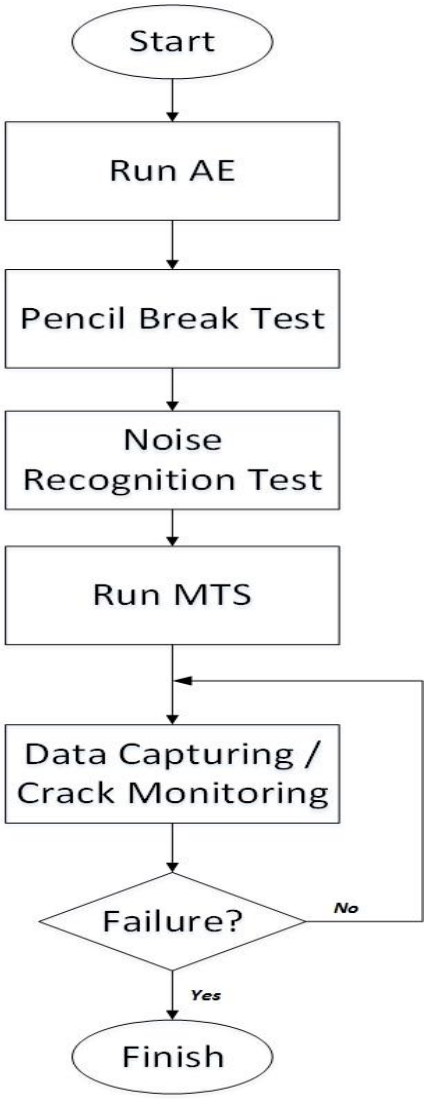

Figure 3.4 Experimental procedure flowchart

4 RESULTS AND ANALYSIS

Experimental results regarding both the energy method and acoustic emission were processed and analyzed individually using MATLAB software. Results from each of the two types of testing will be shown individually and then combined for further analysis.

4.1 Energy method results

Fatigue tests were conducted at several stress levels for comparison between various fatigue lives. The two main goals of this testing (for hysteresis energy) was to determine the total accumulated hysteresis energy and the steady state hysteresis energy value for each stress level. Because all fatigue tests last for a different number of cycles, the results are plotted on a normalized cycle axis. In a normalized cycle axis, the actual cycle number is divided by total number of cycles to failure; thus, the normalized axis is between 0 and 1.

Accumulated hysteresis energy values (on a normalized life axis) are shown in Figure 4.1, Figure 4.2 and Figure 4.3.

Table 4.1, Table 4.2 and Table 4.3 summarize results regarding the accumulated hysteresis energies at different stress levels. As shown in these tables, the standard deviations for the accumulated hysteresis energy are relatively small (when considering the variability of fatigue results). This is encouraging because this testing was the first known strain energy fatigue testing on notched flat rectangular cross sectioned specimen. This information will be used with the steady state hysteresis energy values to predict the fatigue life of the specimens.

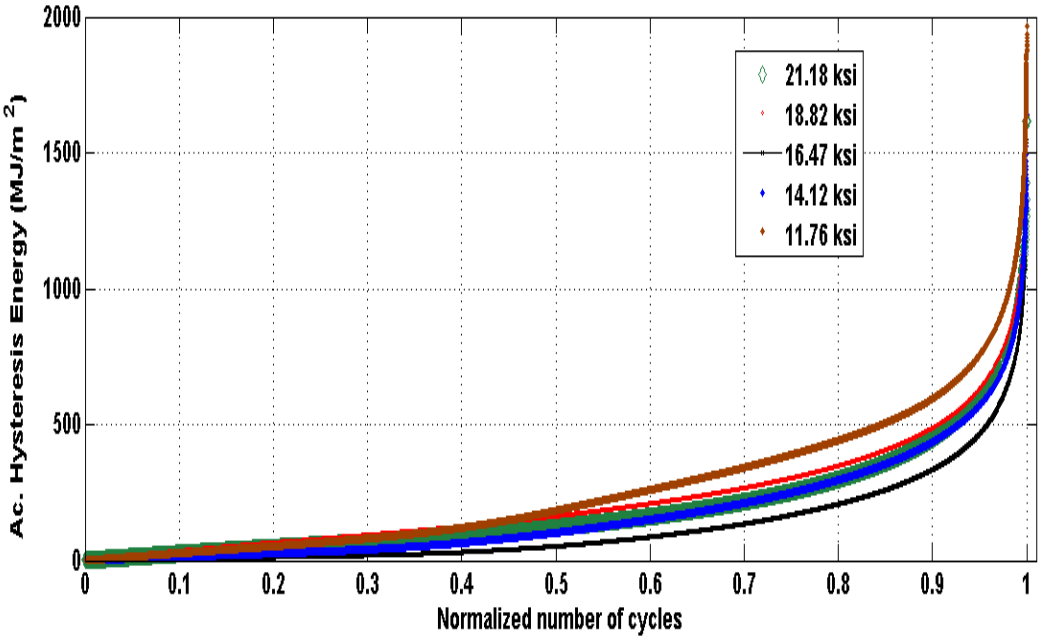

Figure 4.1 Accumulated Hysteresis Energy Vs. Normalized Cycles (Al6061-T6- Style A)

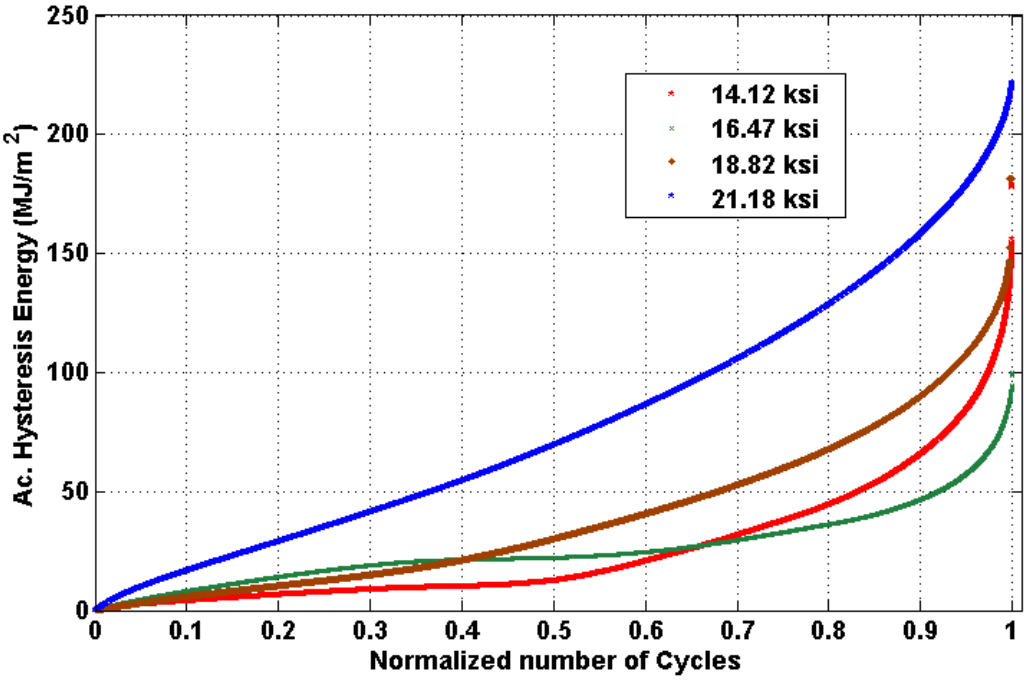

Figure 4.2 Accumulated Hysteresis Energy Vs. Normalized Cycles (Al7075-T6)

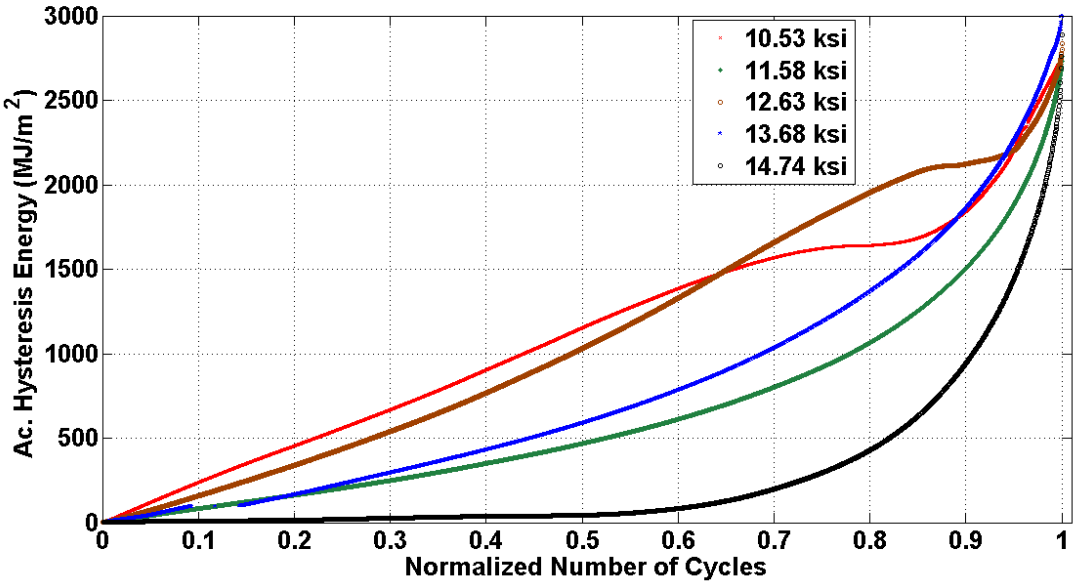

Figure 4.3 Accumulated Hysteresis Energy Vs. Normalized Cycles Al6061-T6- Style B

Next, the hysteresis energy was analyzed on a normalized cyclic basis for the same testing as shown above. The reason for this analysis is to determine the steady state hysteresis strain energy values which will be used for the fatigue predictions. Data is plotted in the Figure 4.4, Figure 4.5 and Figure 4.6 for these tests.

Table 4.1 summary of the results for Accumulated Hysteresis Energy (Al 6061-T6 -Style A)

Stress Level (ksi)	Accumulated Hysteresis Energy (MJ/m^2)	# of cycles to failure
11.76	1648	46806
14.12	1641	21359
16.47	1619	12168
18.82	1549	7662
21.18	1540	5015
STD DEV	42.92	
Average	1599.4	

Table 4.2 summary of the results for Accumulated Hysteresis Energy (Al 7075-T6)

Stress Level (ksi)	Accumulated Hysteresis Energy (MJ/m^2)	# of cycles to failure
16.47	178.8	14088
18.82	181.7	8769
21.18	221.9	5378
STD DEV	24.09	
Average	194.13	

Table 4.3 summary of the results for Accumulated Hysteresis Energy (Al 6061-T6- Style B)

Stress Level (ksi)	Accumulated Hysteresis Energy (MJ/m^2)	# of cycles to failure
10.53	2747	9803
11.58	2758	5995
12.63	2832	5426
13.68	2996	3657
14.74	2886	2234
STD DEV	56.70	
Average	2843.8	

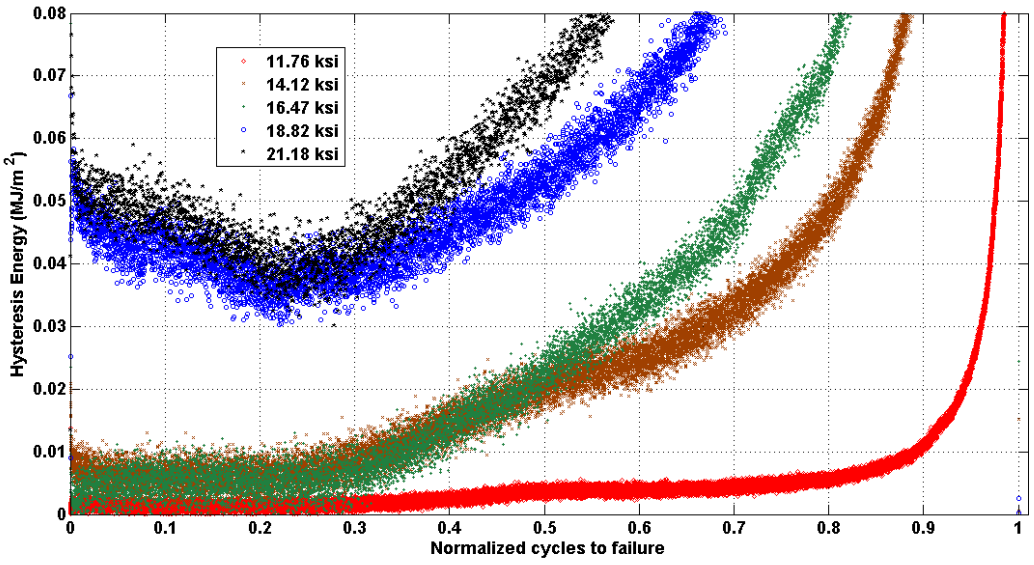

Figure 4.4 Hysteresis Energy Vs. Normalized Cycles Al6061-T6 – Style A

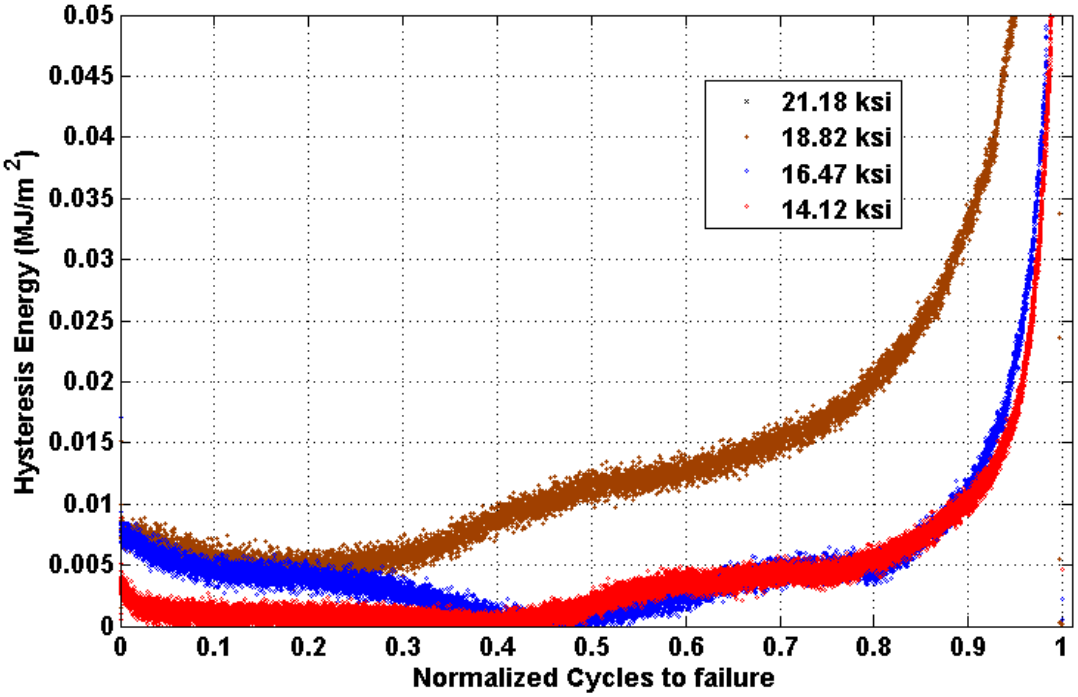

Figure 4.5 Hysteresis Energy Vs. Normalized Cycles Al7075-T6

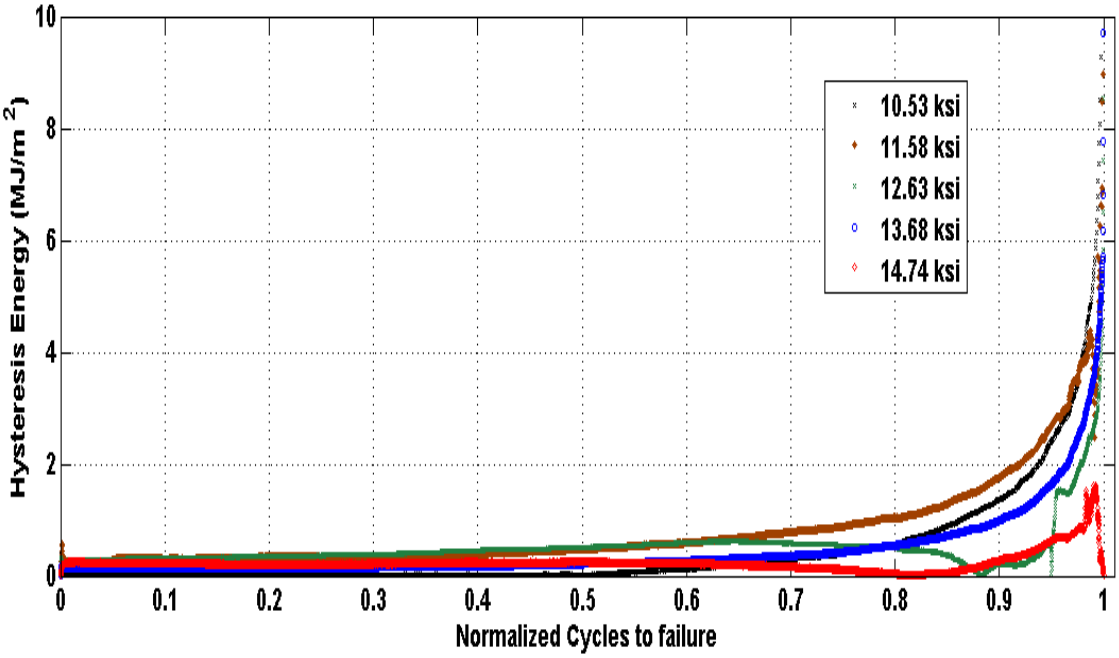

Figure 4.6 Hysteresis Energy Vs. Normalized Cycles Al6061-T6- Style B

The new approach is applied to hysteresis energy values. After calculating the average of α values, the estimated cycles are predicted. The estimated results were then compared with the experimental ones to show the accuracy of the proposed model. These results have been shown in Figure 4.7, Figure 4.8 and Figure 4.9 in a typical S-N curve. Table 4.4 shows the regression lines using the average of α values and the R- squared values. The R-squared values are more than 90 percent which shows the accuracy of the regression and how well the predicted model could be used compared with the experimental results.

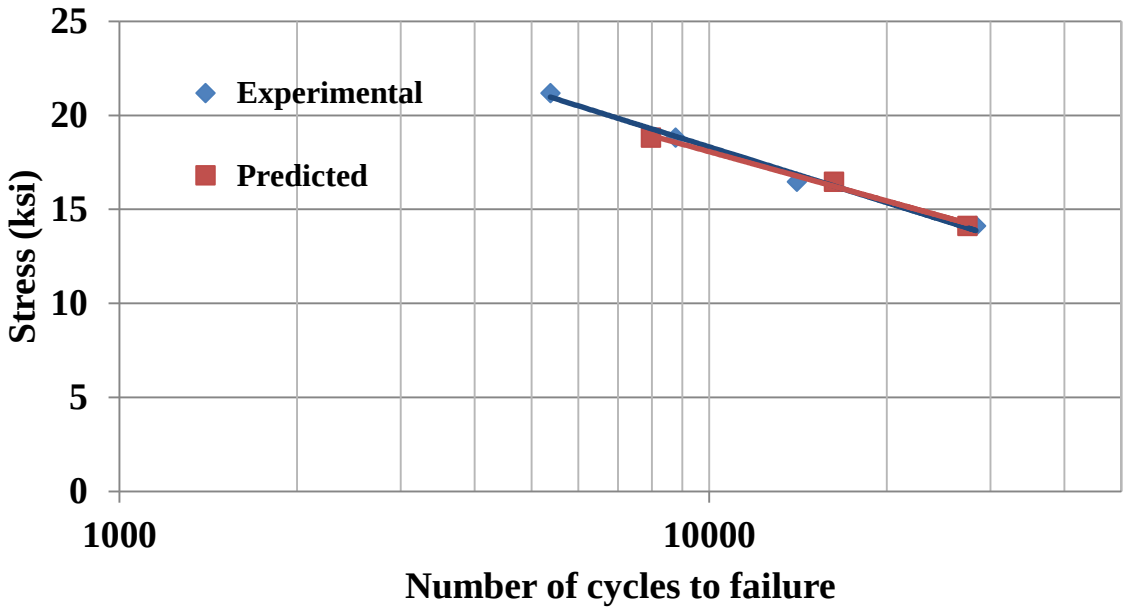

Figure 4.7 Comparison between the experimental and estimated S-N curve for Al 7075-T6

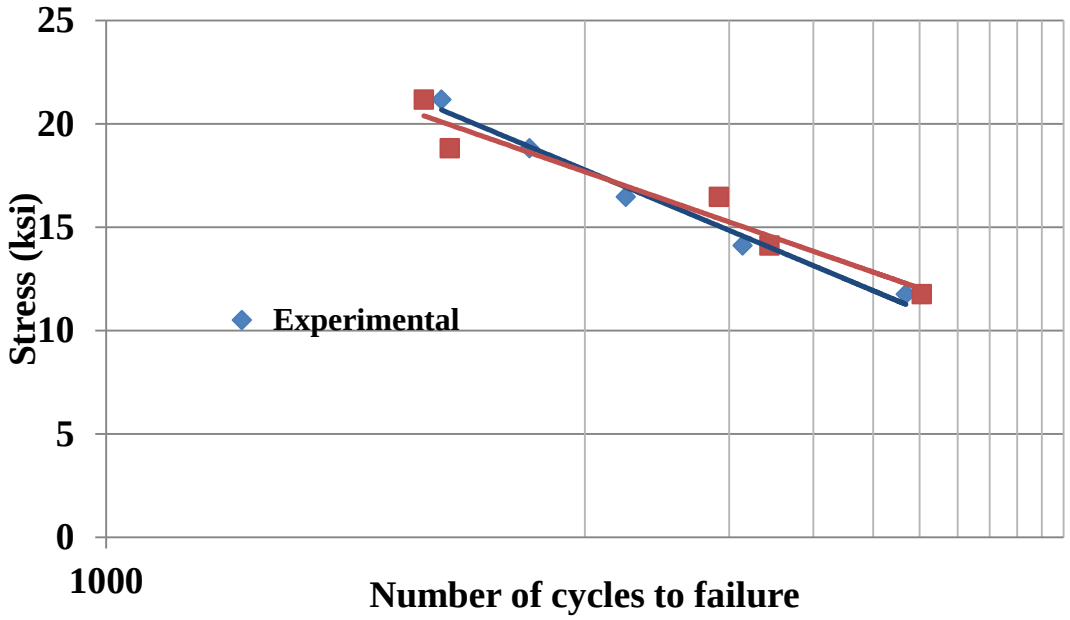

Figure 4.8 Comparison between the experimental and estimated S-N curve for Al 6061-T6 – Style A

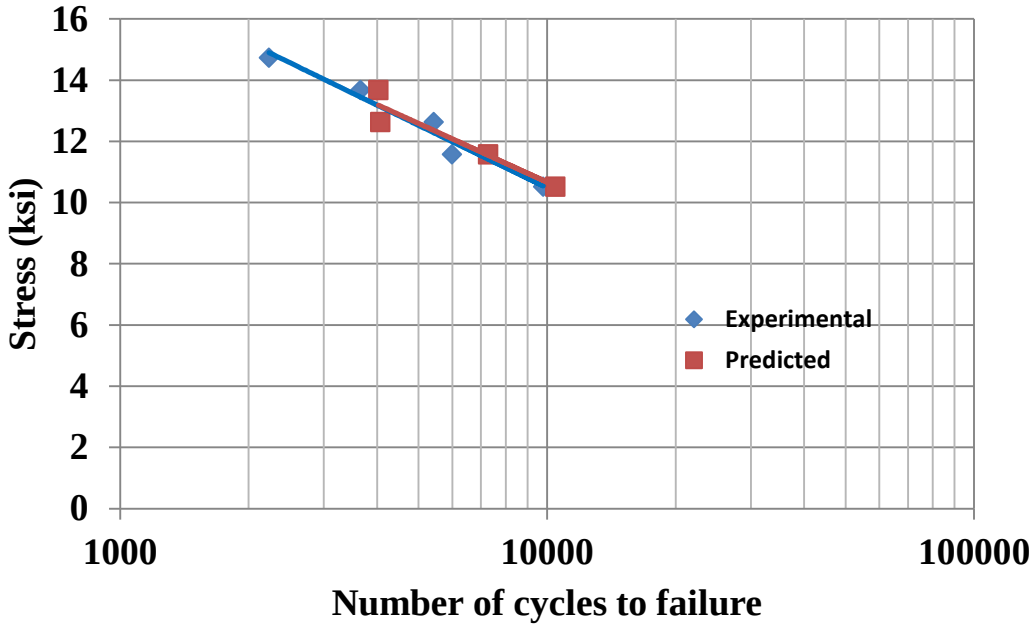

Figure 4.9 Comparison between the experimental and estimated S-N curve for Al 6061-T6- Style B

Table 4.4 Regression coefficients with R-squared values of Predicted cycles

Stress Level	Regression line	R-squared
Aluminum 7075-T6	y = -3.78ln(x) + 52.883	0.9918
Aluminum 6061-T6 Style A	y = -3.5ln(x) + 49.913	0.9412
Aluminum 6061-T6 Style B	y = -4.29ln(x) + 56.042	0.905

The calculation of estimated number of cycles to failure, based on the minimum and maximum values of α, is an indicator for the prediction range of this approach. The estimated S-N curve values were also plotted with the prediction ranges in Figure 4.10, Figure 4.11 and Figure 4.12 to show the accuracy of the correlation for the whole life cycle.

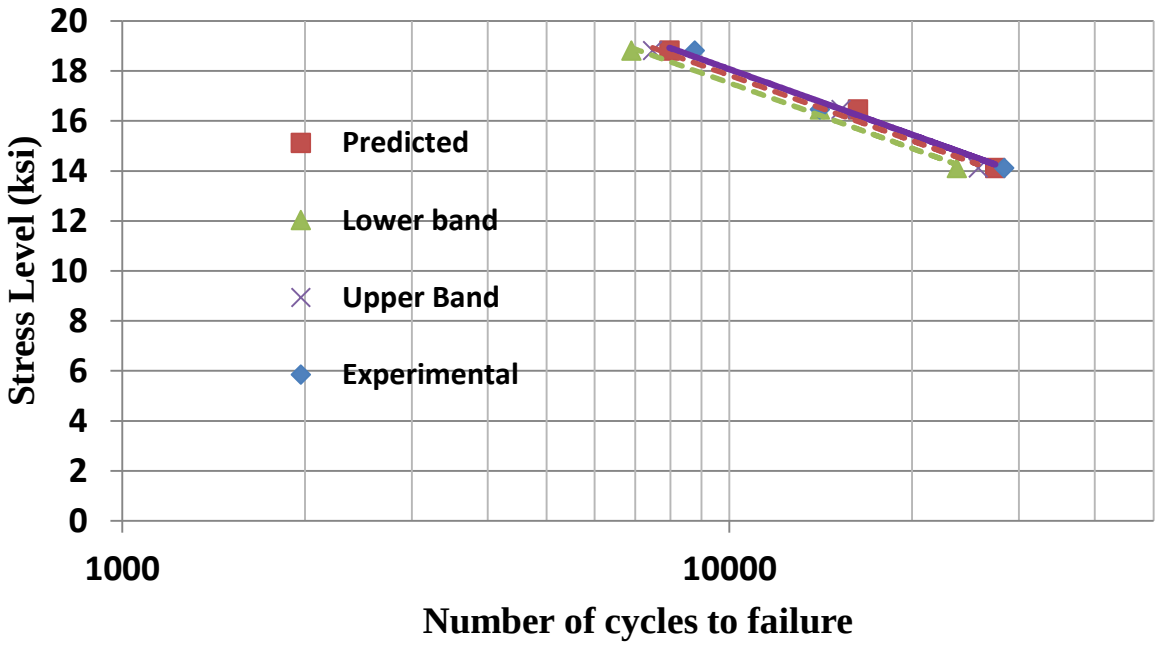

Figure 4.10 Experimental and estimated S-N curve with error bands for Al 7075-T6

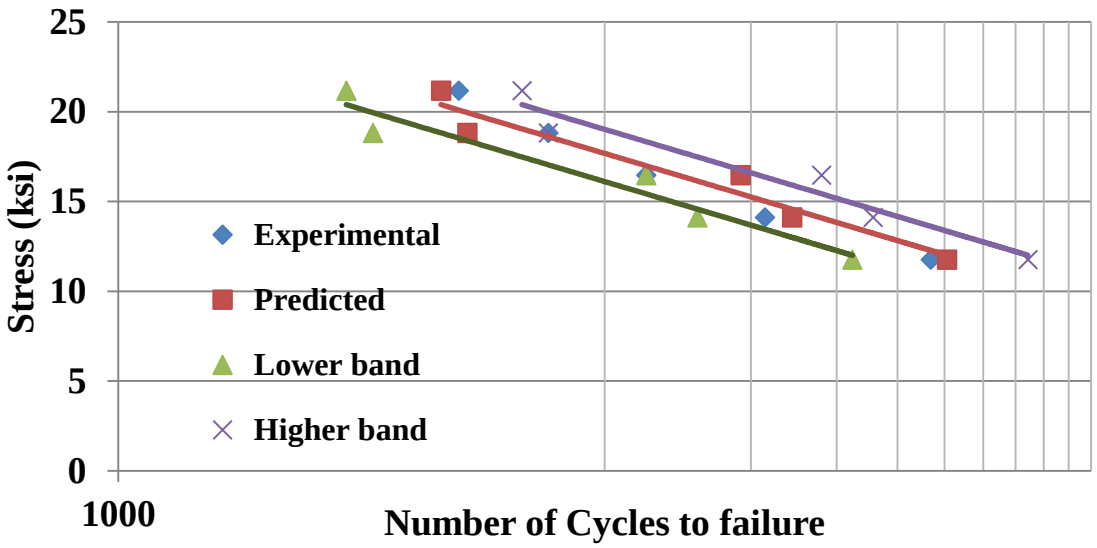

Figure 4.11 Experimental and estimated S-N curve with error bands for Al 6061-T6 – Style A

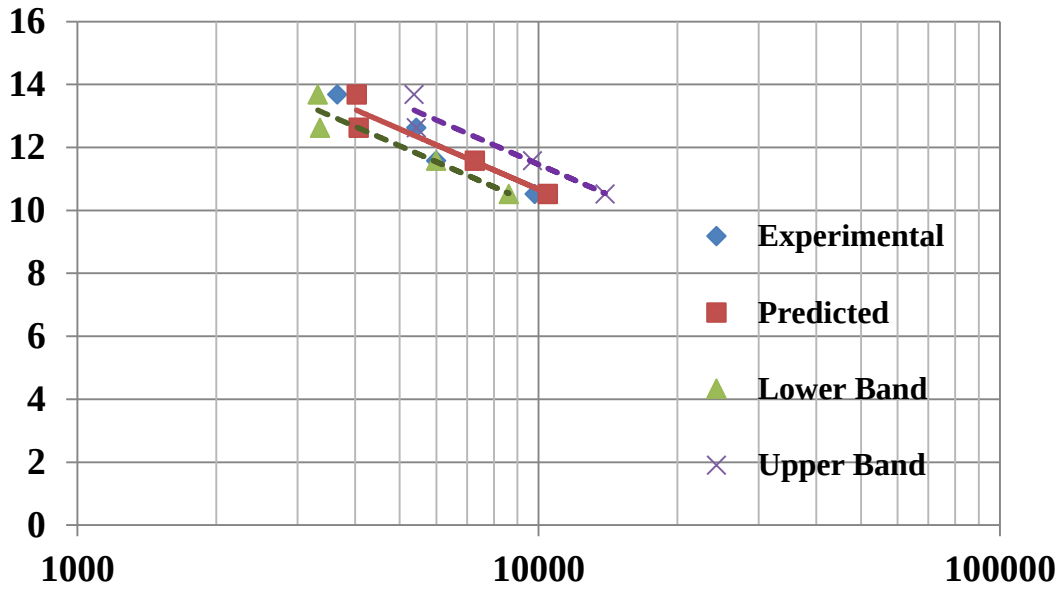

Figure 4.12 Experimental and estimated S-N curve with error bands for Al 6061-T6 – Style B

4.2 Acoustic emission results

The Table 4.5 and Table 4.6 summarized the statistical dependencies of two important variables in strain energy method, hysteresis energy with the acoustic emission energy for two different notch and geometry sizes of aluminum 6061-T6 in load cycles. As it can easily be seen the high values of Spearman coefficients (around 70 percent for aluminum 6061-T6 Style A and Style B) and low values of standard deviations certify the applicability of the energy method to acoustic emission energy.

Table 4.5 Spearman Correlation analysis between Hysteresis Energy & Acoustic Energy (Al 6061-T6-Style A)

Load Level	Stress Level (ksi)	Spearman
3000	14.12	0.56
3500	16.47	0.87
4000	18.82	0.61
4500	21.18	0.73
	STD DEV	0.12
	Average	0.69

Table 4.6 Spearman Correlation analysis between Hysteresis Energy & Acoustic Energy (Al 6061-T6 -Style B)

Load Level	Stress Level (ksi)	Spearman Correlation
2750	11.58	0.57
3000	12.63	0.54
3250	13.68	0.83
3500	14.74	0.87
	STD DEV	0.15
	Average	0.70

The same strategy as the strain energy method was applied to the acoustic emission datasets. One of the major differences is the scattered nature of the acoustic data points (acoustic emission events do not happen at guaranteed time/cycle intervals). Due to the existence of noise in the acoustic emission signal resulting in extreme outliers in the outputs, the acoustic emission energy values were smoothed using a 1st order filter built into MATLAB. The average accumulated acoustic emission energy for each of the stress levels tested was used as total accumulated energy value. In order to obtain the "steady state" energy value, a standard rule was developed to use the median of the 50 percent of the specimen's lifetime. The median was instead of average for the steady state acoustic energy calculations because the median is used in skewed distributions and especially when there are measurement errors [30].

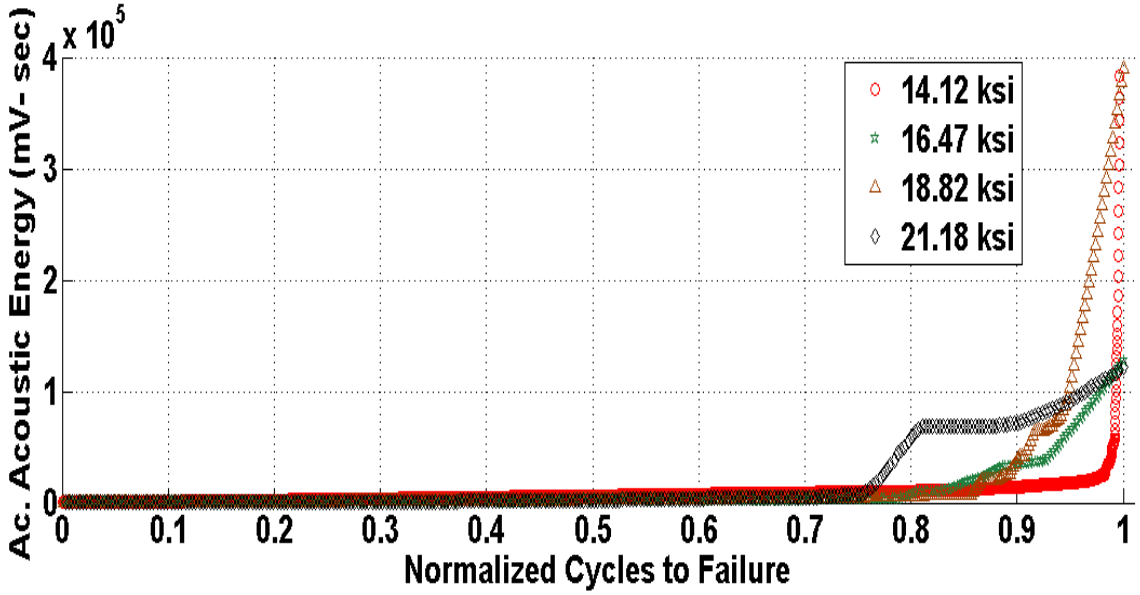

Figure 4.13 Accumulated Acoustic Energy Vs Normalized Cycles (Al 6061-T6- Style A)

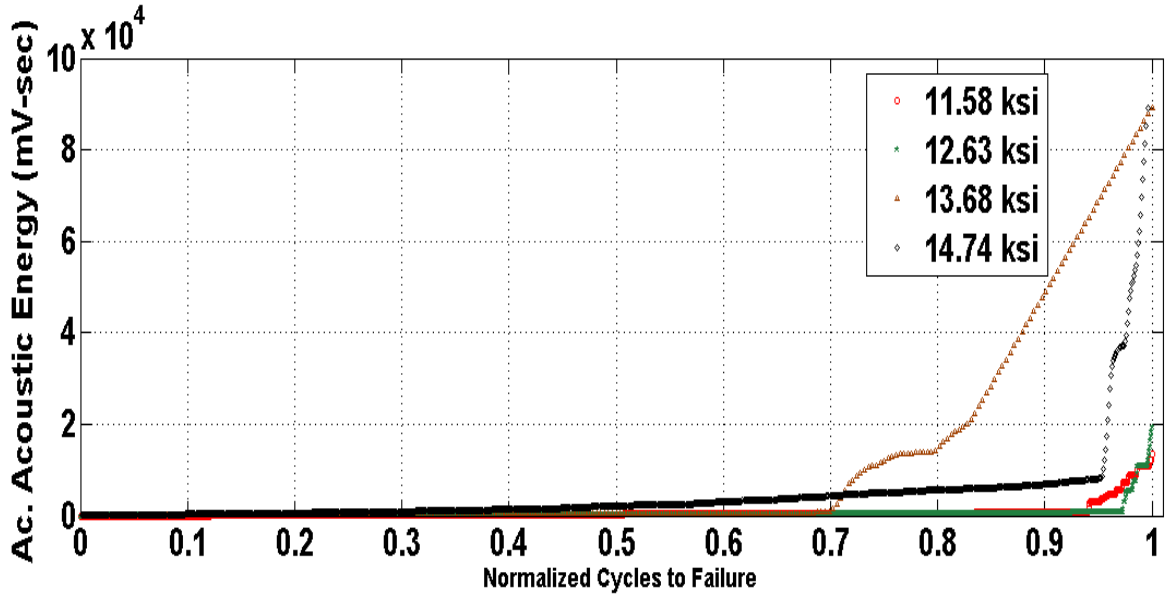

Figure 4.14 Accumulated Acoustic Energy Vs Normalized Cycles (Al 6061-T6- Style B)

Figure 4.13 and Figure 4.14 show the accumulated acoustic energies versus the normalized cycles (normalized event time) to failures for all stress levels for both notch sizes of aluminum samples (Style A and Style B). As it can be seen, the end values of accumulated acoustic energies are equal by pairs for both styles A and B. Therefore taking the average values of the accumulated acoustic energies seems promising and logical. The average values of the final accumulated energies were taken for the prediction analysis.

Table 4.7 and Table 4.8 summarized the numerical results from the accumulated acoustic energies for two aluminum 6061-T6 style A and B designs.

Table 4.7 Summary of the results for Accumulated Acoustic Energy

(Aluminum 6061-T6-Style A)

Stress Level (ksi)	Ac. Acoustic Energy (mV- sec)	# of cycles to failure
14.12	3.84E+05	29000
16.47	1.27E+05	10900
18.82	3.91E+05	6380
21.18	1.22E+05	5300
STD DEV	136394	
Average	2.56E+05	

Table 4.8 Summary of the results for Accumulated Acoustic Energy

(Aluminum 6061-T6-Style B)

Stress Level (ksi)	Ac. Acoustic Energy (mV- sec)	# of cycles to failure
17.95	1.79E+04	46806
19.58	1.73E+04	21359
21.21	8.92E+04	12168
22.84	8.92E+04	7662
STD DEV	39382	
Average	5.34E+04	

Figure 4.15 and Figure 4.16 show the acoustic emission energies versus normalized cycles (normalized event time) to failure for both aluminum 6061-T6 style A and B designs. As it can be seen in Table 4.9 and Table 4.10, Median values of these stress levels for the 50 percent of life cycles were calculated and used for the prediction phase.

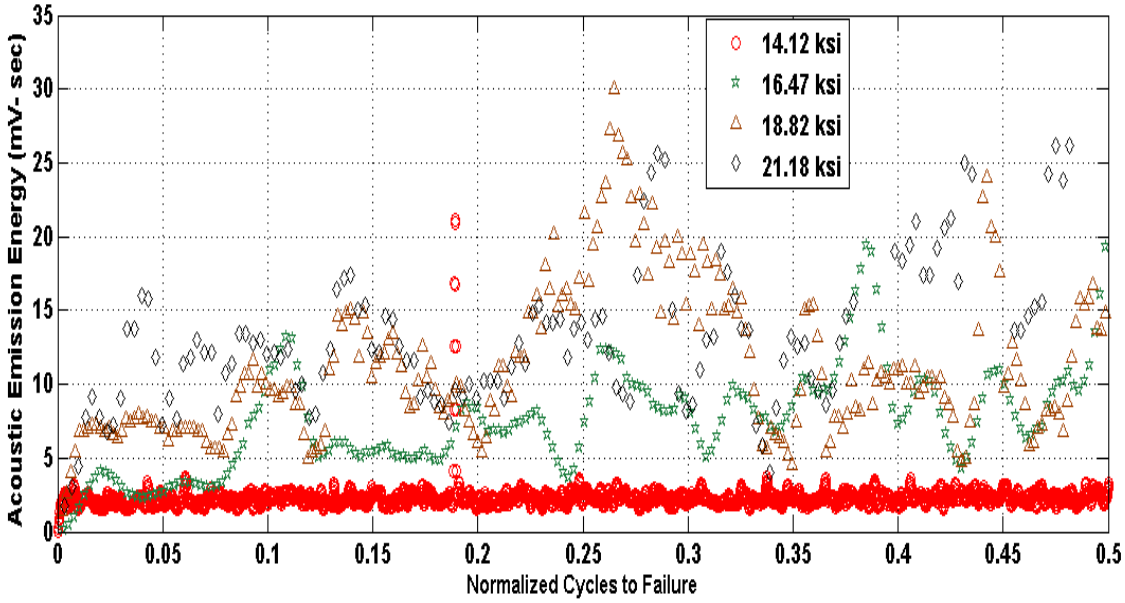

Figure 4.15 Acoustic Energy Vs Normalized Cycle (Al 6061-T6- Style A)

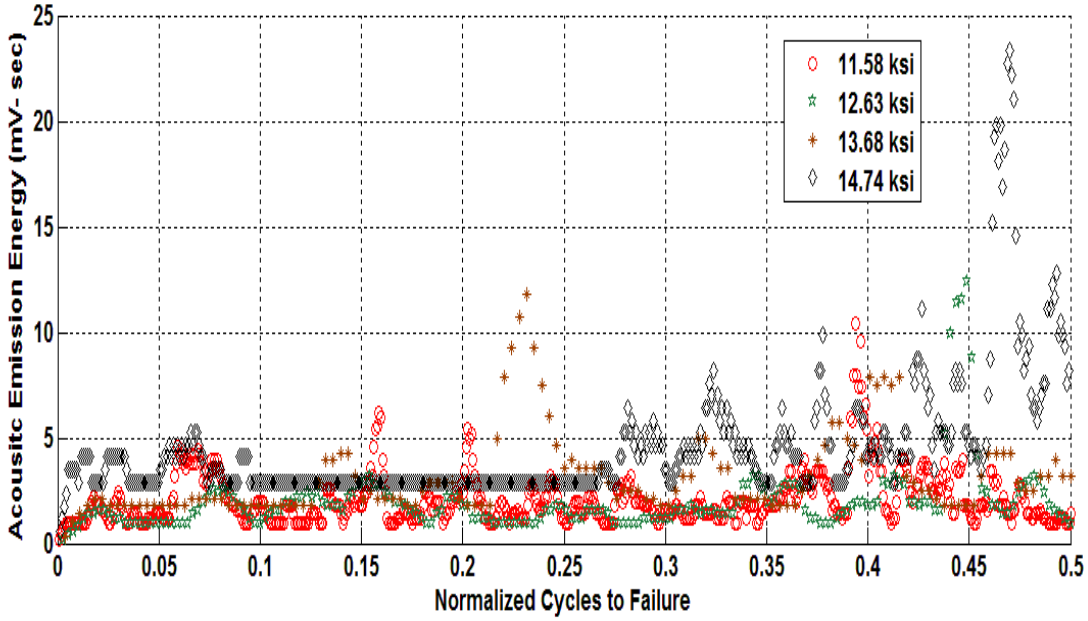

Figure 4.16 Acoustic Energy Vs Normalized Cycle (Al 6061-T6- Style B)

Table 4.9 Summary of the Median values for each test for Al 6061-T6 Style A

Stress Levels	Median values
14.12	2.16
16.47	5.7323
18.82	9.8
21.18	11.8

Table 4.10 Summary of the Median values for each test for Al 6061-T6 Style B

Stress Levels	Median values
17.95	1.8
19.58	1.6
21.21	2.5
22.84	3.5

With the previous information, life predictions can now be made using Equation 2.11. The results were then compared with the experimental data points as shown in Figure 4.17 and Figure 4.18 on S-N curves.

As it can be seen from the Table 4.11, the high values of R-squared for both styles A and B assure the applicability of the energy method to the acoustic emission technique.

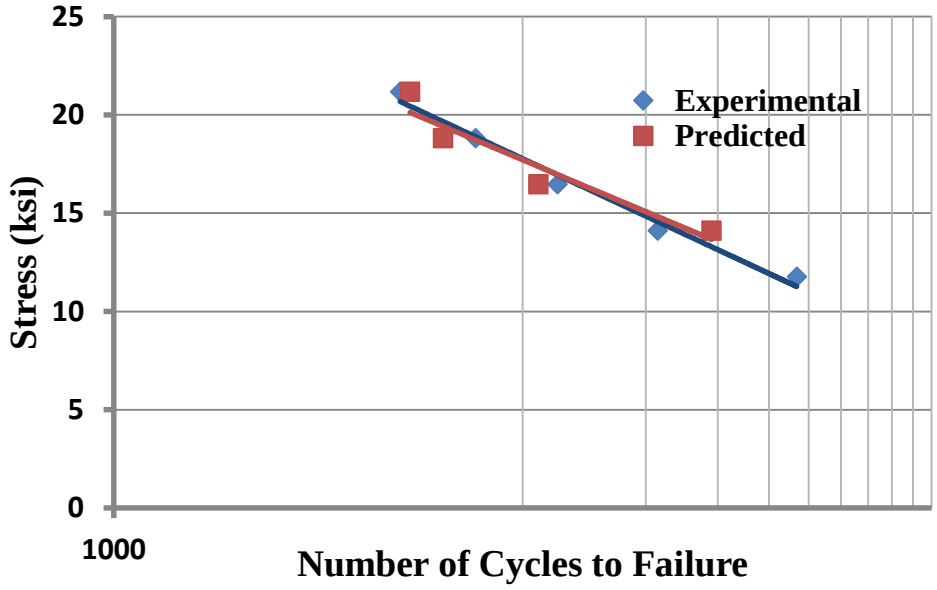

Figure 4.17 Comparison between the experimental and estimated S-N curve for Al 6061-T6- Style A

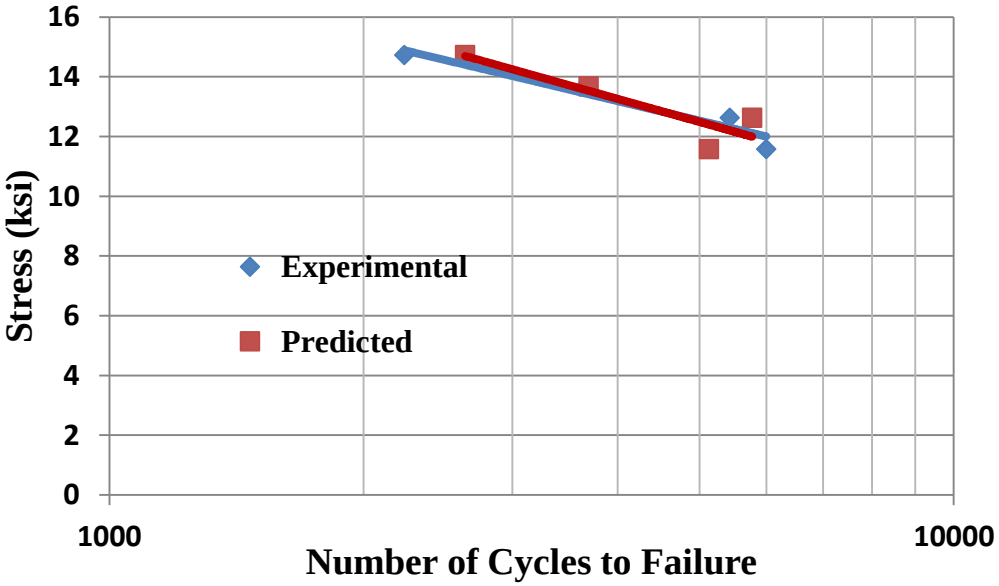

Figure 4.18 Comparison between the experimental and estimated S-N curve for Al 6061-T6- Style B

Table 4.11 Regression coefficients with R-squared values of Predicted cycles

Material Type	Regression line	R-squared
Aluminum 6061-T6 Style A	y = -4.532ln(x) + 54.941	0.9165
Aluminum 6061-T6 Style B	y = -5.3497ln(x) + 61.2156	0.8004

Similar to hysteresis energy calculations, the estimated S-N curve values were also plotted with the prediction ranges in Figure 4.19 and Figure 4.20 to show the accuracy of the correlation for whole life cycle.

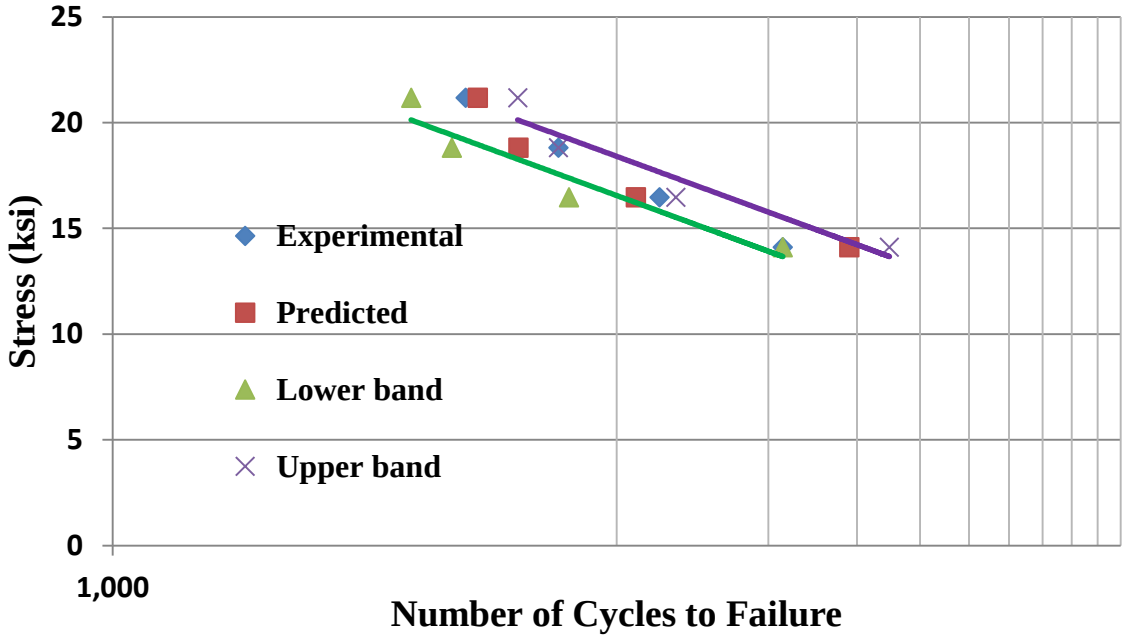

Figure 4.19 Experimental and estimated S-N curve with error bands for Al 6061-T6 – Style A

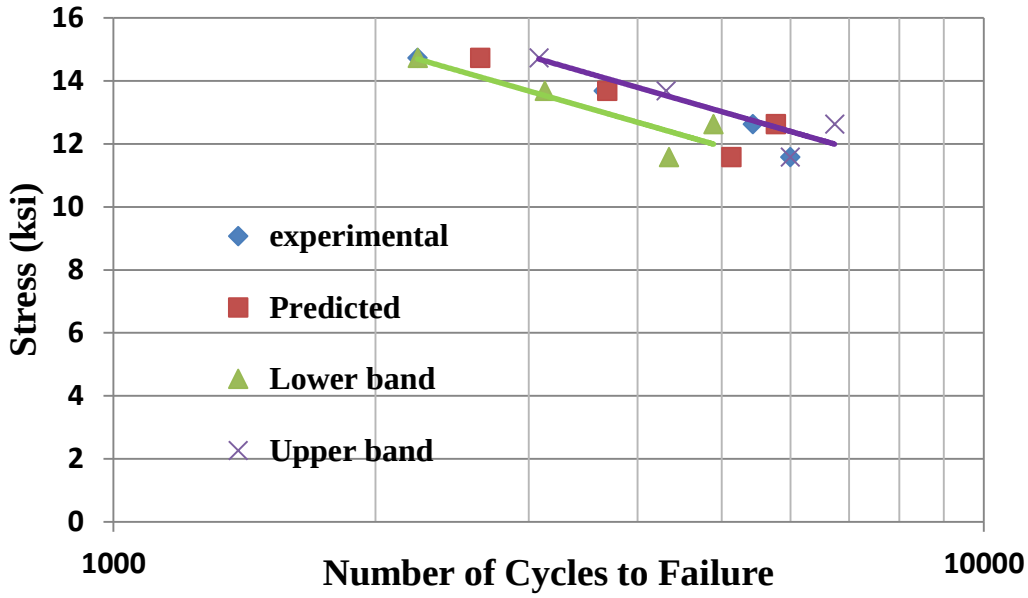

Figure 4.20 Experimental and estimated S-N curve with error bands for Al 6061-T6 – Style B

Similar to the strain energy method, using acoustic emission energy values to determine fatigue life is a fairly quick and reliable method for making simple predictions.

4.3 Comparison between hysteresis energy with acoustic emission energy

A Statistical analysis was used to compare hysteresis energy and acoustic energy. In Table 4.12 through Table 4.15, the estimated and experimental cycles for different stress levels were compared by means of percentage of errors. Except for two of stress levels for calculation of percentage of errors in comparison between estimated cycles and experimental cycles, the rest of the values are below 25 percent. Extensometer saturation and other instrumentation errors during the test are the main reasons for the high values of errors. As shown in Table 4.12 and Table 4.13, the average percentage of error for Al 6061-T6- style A, using the hysteresis energy values, was around 24 and this value for aluminum 6061-T6 style B was around 16. Reviewing the similar results, using the

acoustic emission energies were summarized in Table 4.14 and Table 4.15. The average error values of the comparison between the experimental and predicted cycle to failure for Al 6061-T6 applied to both style A and B are around 17 and 11 percent.

Table 4.12 Comparison between Estimated cycle and Experimental Cycles with average error percentage- Hysteresis Energy -Al 6061- T6-Style A

Stress Level	Experimental Cycles	Estimated Cycles	% error
11.76	46806	50559	8.018
14.12	21359	24291	13.73
16.47	12168	19042	56.49
18.82	7662	5221	31.85
21.18	5015	4607	8.13
		Average error	23.64

Table 4.13 Comparison between Estimated cycle and Experimental Cycles with average error percentage- Hysteresis Energy -Al 6061- T6-Style B

Stress Level	Experimental Cycles	Estimated Cycles	% error
10.53	9803	10464	6.75
11.58	5995	7278	21.41
12.63	5426	4072	24.94
13.68	3657	4031	10.23
14.74	2234	2384	6.74
		Average error	15.83

Table 4.14 Comparison between Estimated cycle and Experimental Cycles with average error percentage Acoustic Energy -Al 6061- T6 –Style A

Stress Level	Experimental Cycles	Estimated Cycles	% error
14.12	2.14E+04	2.90E+04	35.57
16.47	1.22E+04	1.09E+04	10.34
18.82	7.66E+03	6.38E+03	16.72
21.18	5.02E+03	5.30E+03	5.67
		Average error	17.074

Table 4.15 Comparison between Estimated cycle and Experimental Cycles with average error percentage Acoustic Energy -Al 6061- T6 – Style B

Stress Level	Experimental Cycles	Estimated Cycles	% error
11.58	5.99E+03	5129	14.40
12.63	5.43E+03	5767	6.28
13.68	3.85E+03	3693	4.12
14.74	2.24E+03	2638	17.94
		Average error	10.68

The error decreased by almost 23 percent for Al 6061-T6- Style A and 15 percent for Al 6061-T6 – Style B. These results were shown in Table 4.16.

Table 4.16 Comparison between % error between Hysteresis and Acoustic Energy

Method	% error for Al6061-T6 - Style A	% error for Al6061-T6 - Style B
Hysteresis	23.64	15.83
Acoustic Emission	17.07	10.68

5 CONCLUSION

5.1 Summary

Acoustic emission monitoring of the modified energy based fatigue life prediction method was applied to: a) improve the accuracy and applicability of the new cyclic energy theory on single edged notch aluminum 6061-T6 specimens and b) assure the advantages of applying such a method to predict the cyclic life of the samples compared with other classical methods. This study shows the applicability of the energy based fatigue life method to notched single edged specimens and indicated a correlation between the acoustic emission energy and strain hysteresis energy in cyclic testing.

5.2 Future work

More experiments are needed on other types of materials to further investigate the correlation between acoustic emission features and hysteresis energies. Future work should explore:

- Varying material types such as steel and Ti 6Al-4V specimens
- A wide range of geometries and dimensions such as Compact Tension(CT) and Single Edge Tension(SE(T)) specimens with thicker and wider dimensions
- Varying load ranges such as fully reversed load range(R=-1)

6 APPENDIX A: ACOUSTIC EMISSION SETUP

After choosing a layout for each AE test, Acoustic Emission (AE) Hardware parameters for data acquisition must be defined. The following notes will describe the settings used in this thesis.

6.1 AE Hardware Setup

Because two AE sensors are used simultaneously, two acoustic emission channels are selected according to Figure 6.1. Threshold values are chosen according to noise recognition testing. Noise recognition testing is a test conducted while the specimen is locked in the MTS machine grips, with the MTS landmark machine on but not running any test. During this time, the AE system is capturing AE events. The values 40, 45 and 50 dB were set based on the background signal noise transferring from the hydraulic grips to the specimens. As seen in Figure 6.1, the pre-amplified gain value was set to 40 dB. The analogue filters were in the range between 200 KHz and 400 KHz. Experiments have shown that frequency range for most background noises is below 200 KHz. The AE system cannot transfer more than 10 MSPS, therefore, 1 and 2 mega samples per second were selected. Appropriate selection of pre-trigger parameter (in microsecond) ensures the software records enough information about the event before the threshold is exceeded. 256 and 512 µsec were chosen for this research. The size of a waveform message is defined as length. According to the Equation 6.1 the appropriate values for these parameters are calculated.

$$time\ length = \frac{No\ of\ kilo\ samples}{Sample\ rate} = \frac{1K}{4MSPS} = \frac{1024x1samples}{4MSPS} = 256\mu s \qquad \text{Equation 6.1}$$

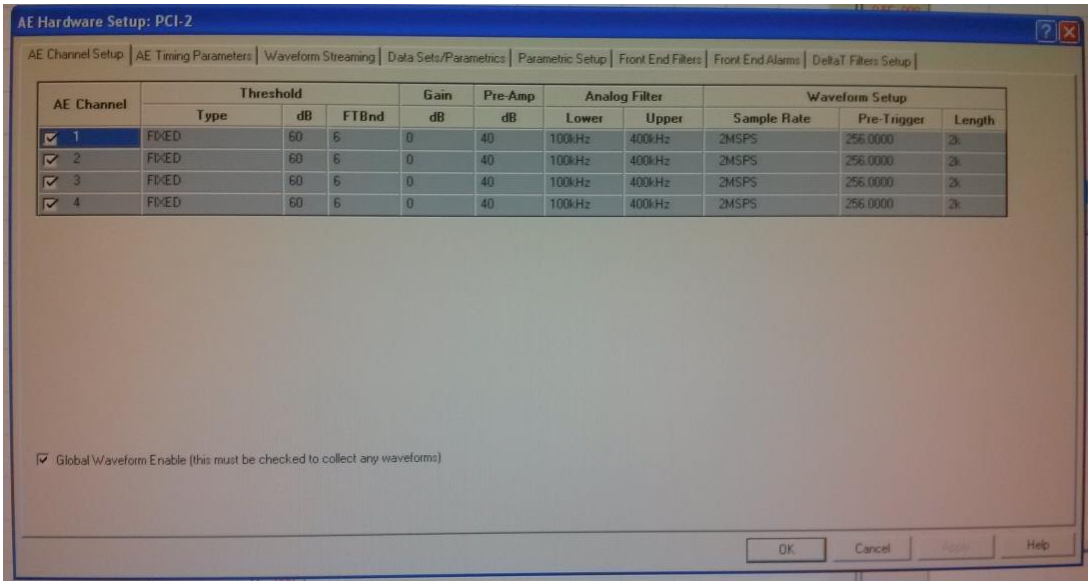

Figure 6.1 AE channel setup

Acoustic emission timing parameters are shown in the Figure 6.2. The appropriate selection of PDT, HDT and HLT are explained in section 3.3 of this thesis.

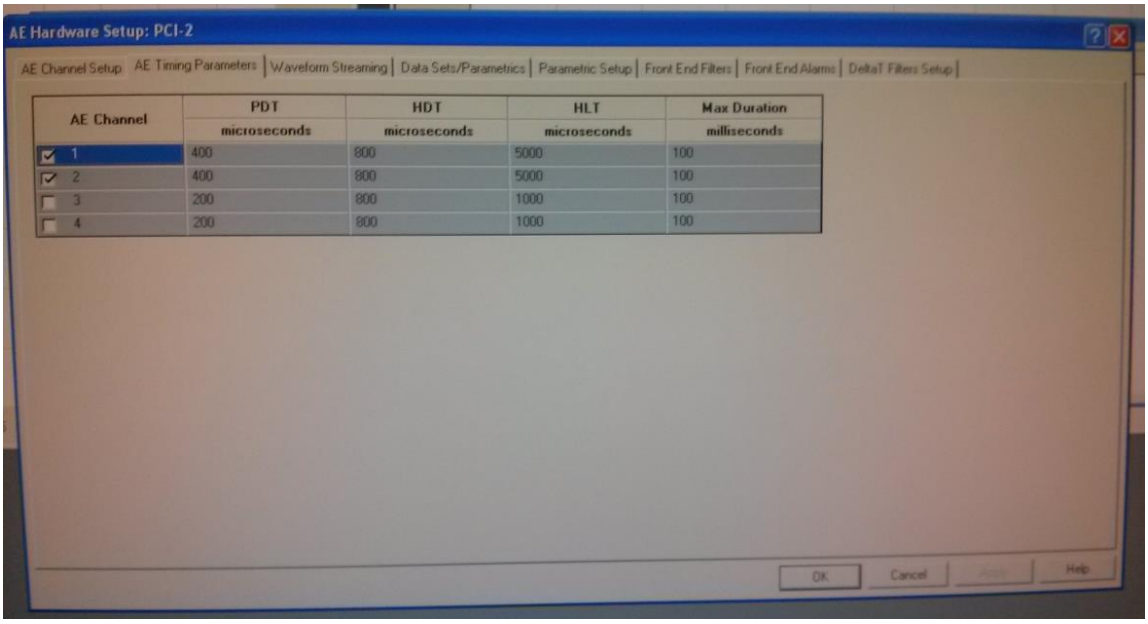

Figure 6.2 AE Timing Parameters

The Hit Data set and parameters are shown in the Figure 6.3. Since the only parametric input is Load, one hit parametric is chosen.

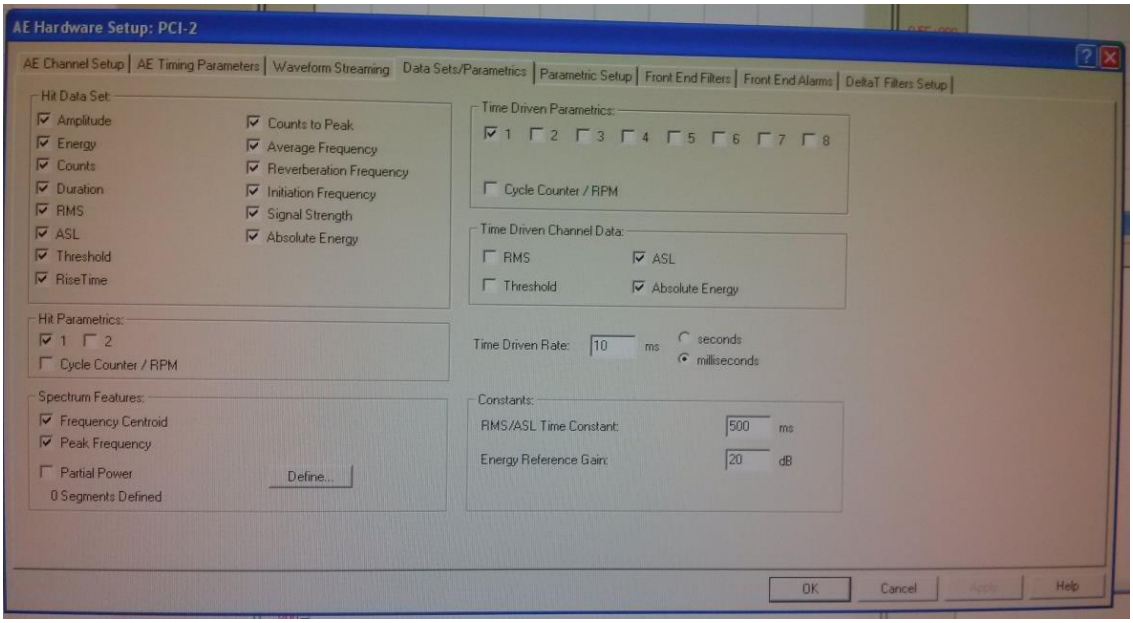

Figure 6.3 Datasets/Parametric

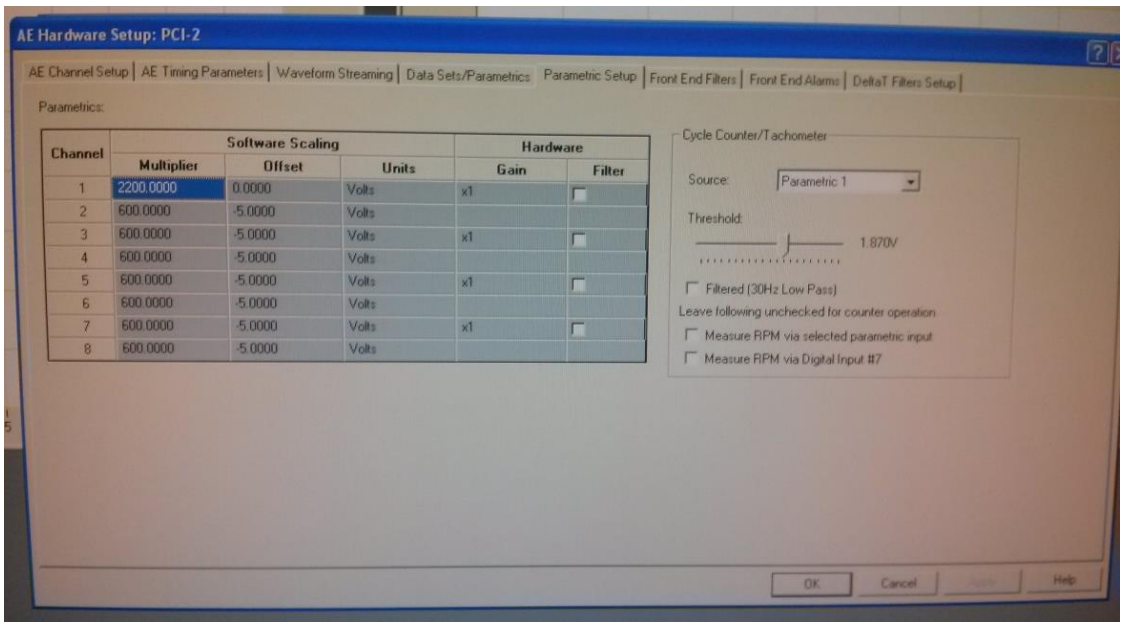

Figure 6.4 Parametric Setup

Parametric setup is shown in Figure 6.4. The multipliers and offset values are set based on the load output values during the test. 2200 is used for the current setup.

Acoustic sensor placement is also defined in AE hardware setup. For this research, AE transducer locations are chosen as linear sources (units are in inches). The longitudinal, shear and surface wave velocities of a typical aluminum specimen are shown in the Figure 6.5. Two average wave velocities have been selected based on material types. Also, the distance between two sensors is defined as Event Definition Value. These units are also defined in inches.

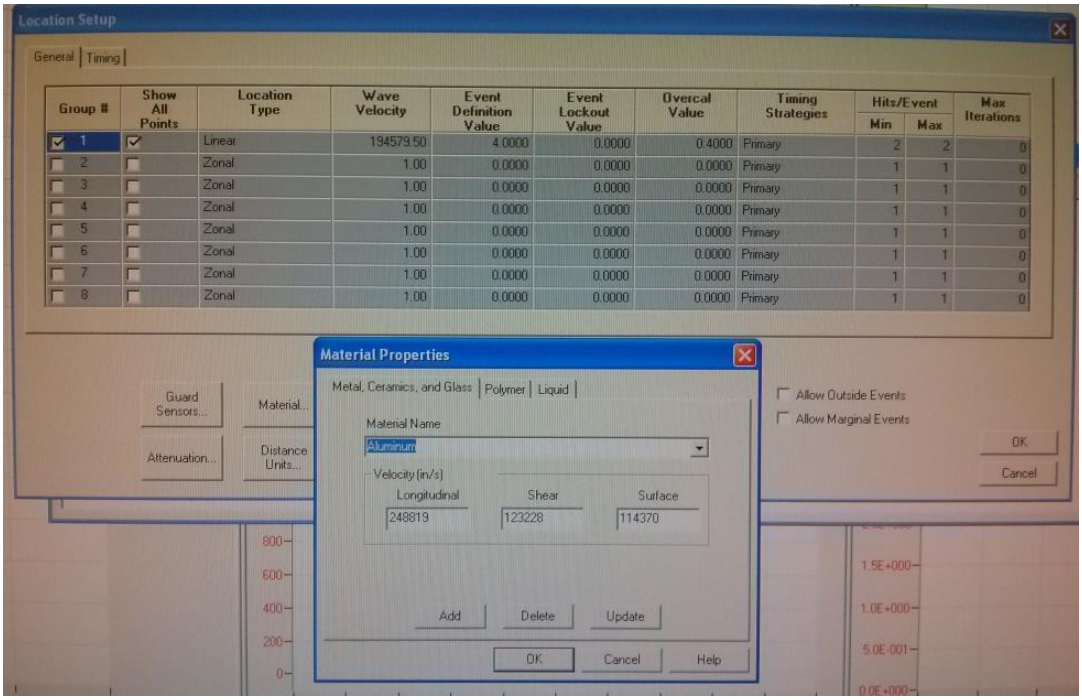

Figure 6.5 Sensor Location Setup

Based on two different styles that are used in this research, sensor placement is defined according to Figure 6.6.

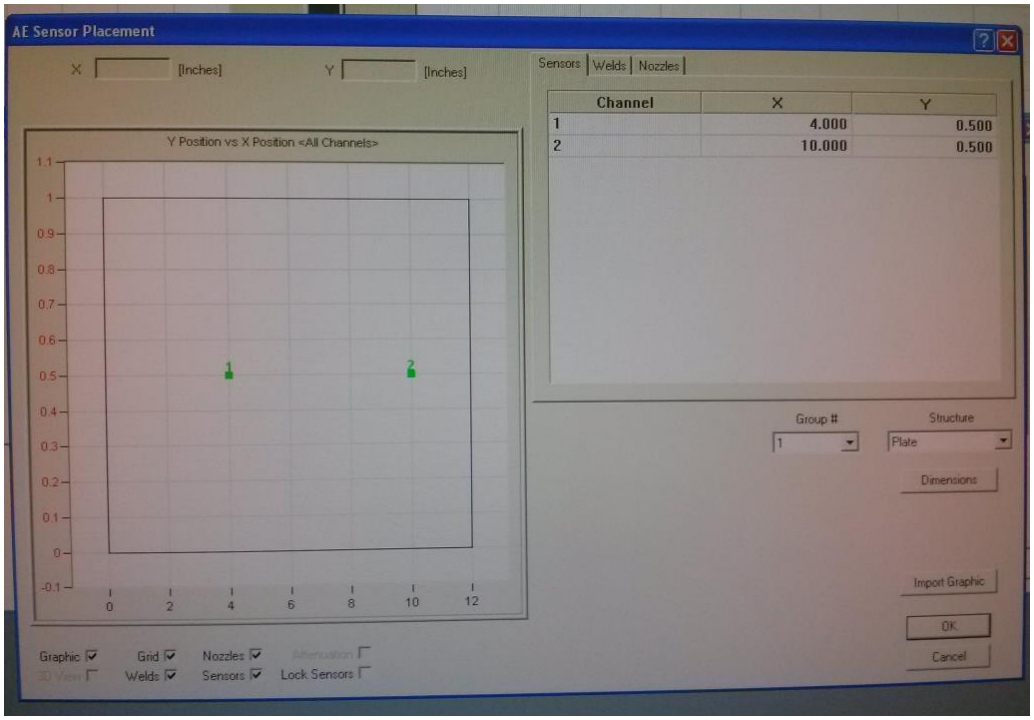

Figure 6.6 AE Sensor Placement

7 APPENDIX B: FATIGUE TESTING SETUP

This appendix describes the setting in the MTS MPT software used to fatigue specimen.

7.1 Fatigue Hardware Setup

After opening the MPT procedure editor as shown in Figure 7.1, use the process palette to set up the test procedure. For this research, the procedures include a ramp procedure (to zero load), a short dwell period, the cyclic procedure and cyclic acquisition to collect stress/strain data.

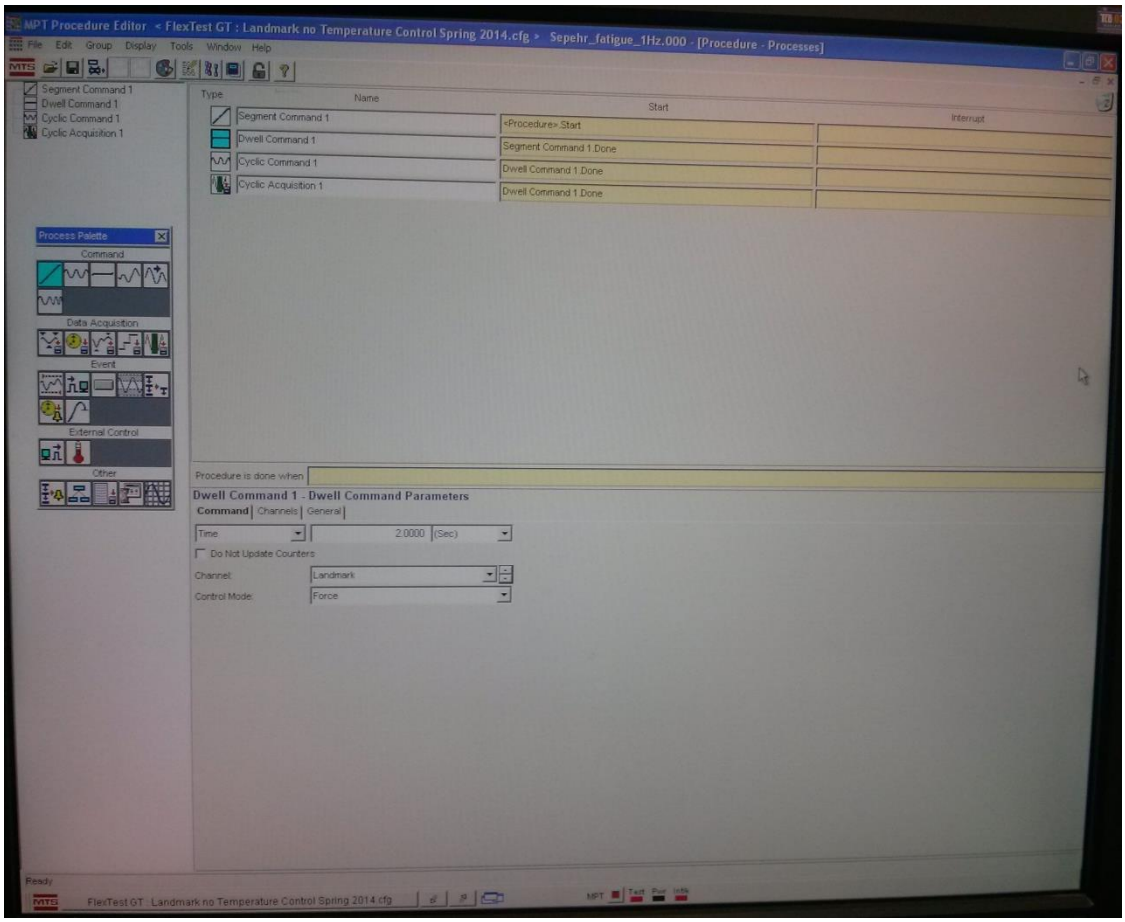

Figure 7.1 Dwelling time setup

Fatigue cycling parameters including segment shape, frequency, adaptive compensator, type of control mode, minimum and maximum load range are defined according to Figure 7.2. As it can be seen, tapered sinusoidal is chosen as segment shape and PVC is set as the adaptive compensator for all tests. Frequency is also set to 2 Hz. The machine is set on force control mode with minimum load equal to zero and maximum load based on Table 3.1.

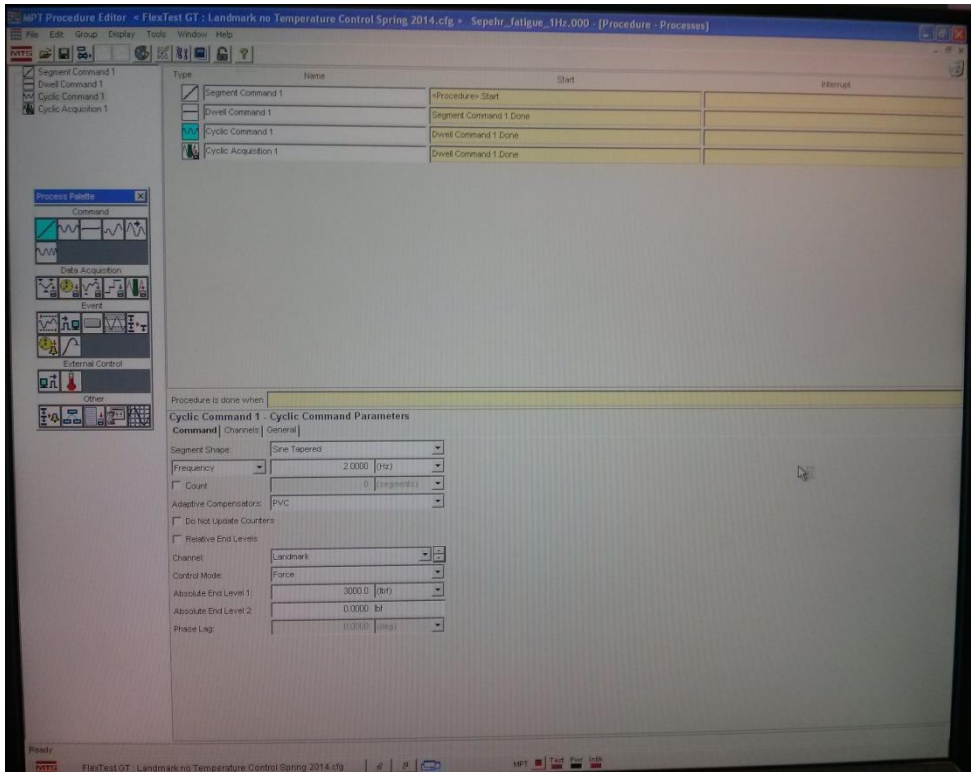

Figure 7.2 Procedure editor

MTS data points are recorded every 2 millisecond according to Figure 7.3.

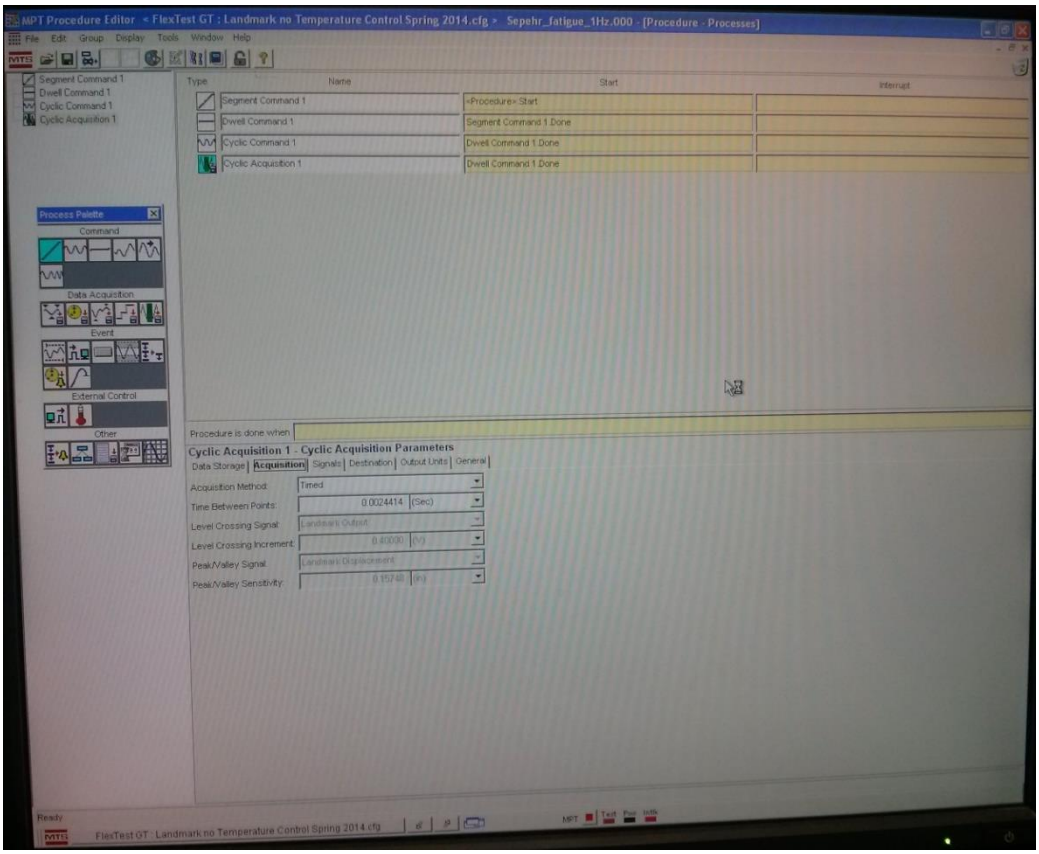

Figure 7.3 Data Acquisition

Total number of cycles that should be recorded is defined according to Figure 7.4. Since Low Cycle Fatigue (LCF) is mostly considered in this research, 100,000 will be enough as the maximum cycle.

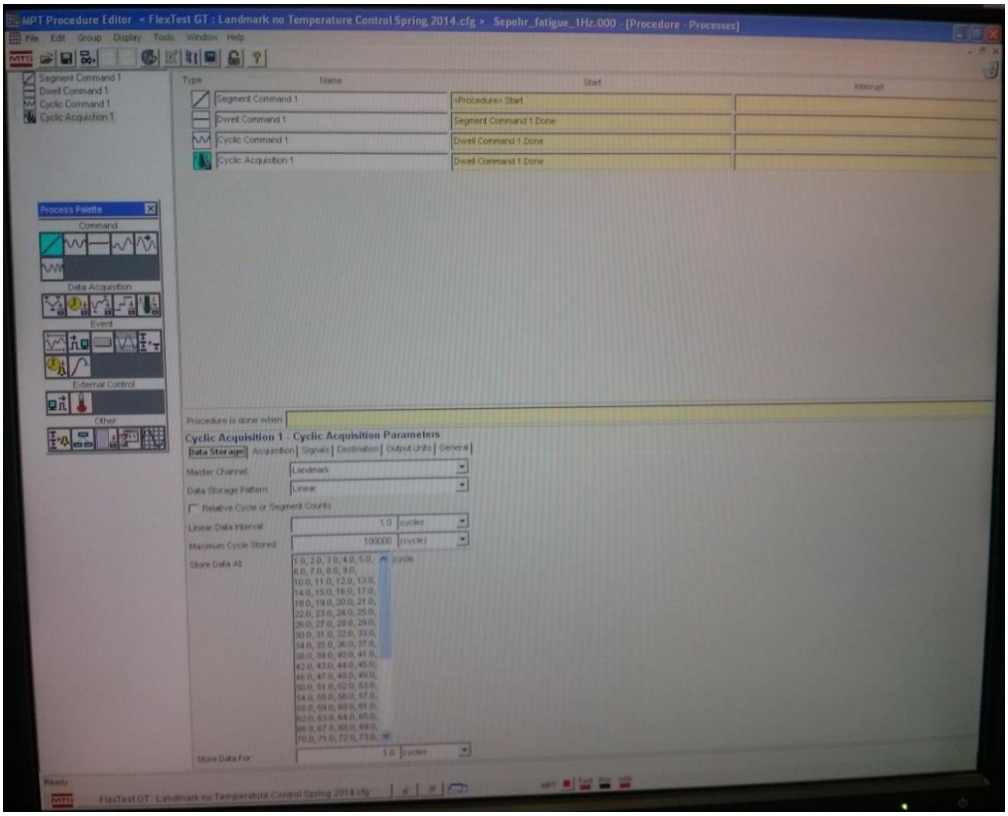

Figure 7.4 Cyclic Acquisition

The output signals that should be recorded during each test are selected according to Figure 7.5 (time, displacement, force and extensometer displacement values).

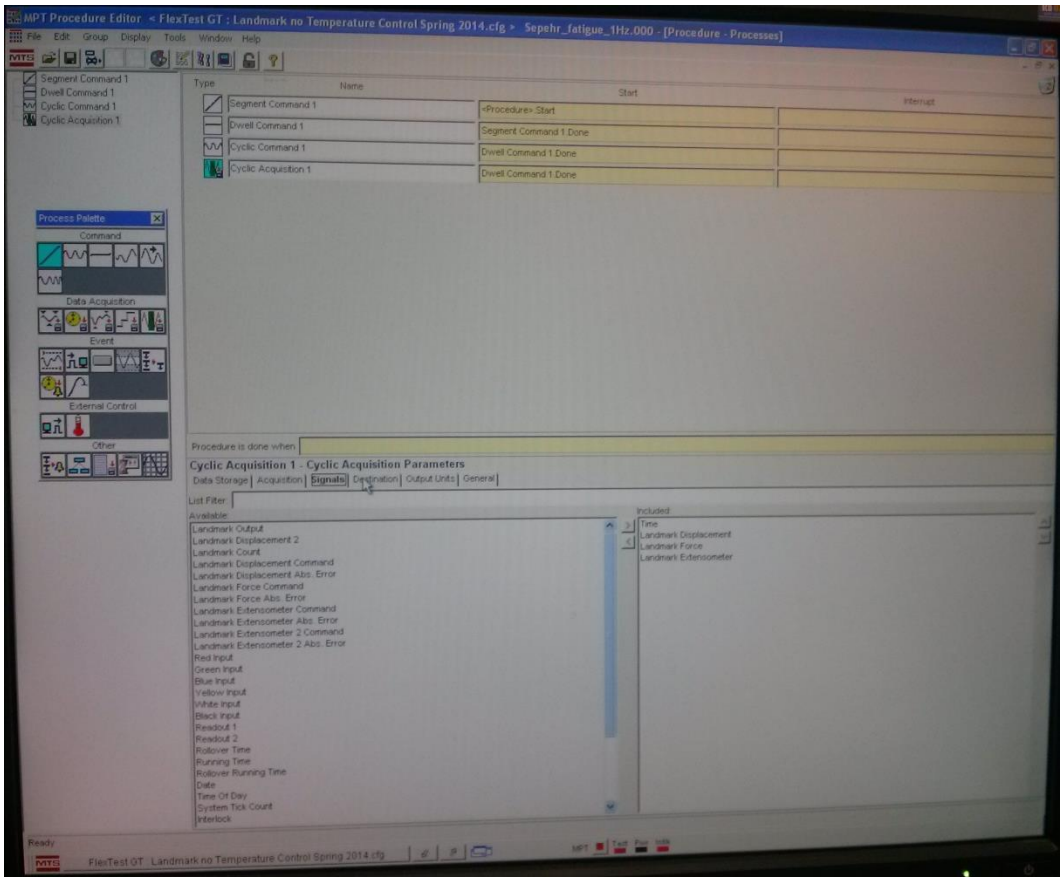

Figure 7.5 output settings

The desired unit is selected according to Figure 7.6. As it can be seen, US unit is defined. It includes force in lbs. and displacement in inches.

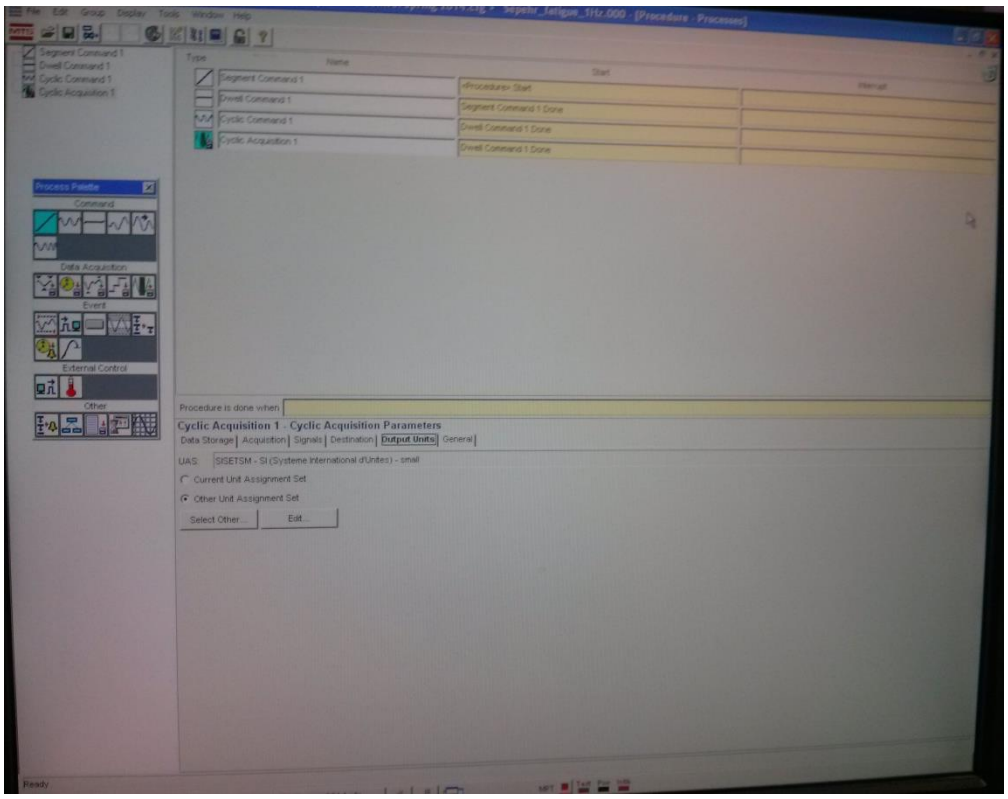

Figure 7.6 Output unit setup

8 BIBLIOGRAPHY

[1] Farahmand, B., 2009, Virtual Testing and Predictive Modeling - For Fatigue and Fracture Mechanics Allowables.

[2] "Mianus River Bridge Collapse" [Online]. Available: http://35wbridge.pbworks.com/w/page/900718/Mianus River Bridge Collapse.

[3] Xu, L. R., "imechanica" [Online]. Available: http://imechanica.org/node/10052.

[4] Scott-Emuakpor, O., George, T., Letcher, T., Shen, M.-H. H., and Cross, C., 2011, "Incorporation of a Probabilistic Monotonic Strain Energy Analysis to a Lifting Method," J. Fail. Anal. Prev., **12**(1), pp. 109–115.

[5] Nesaei, S., Letcher, T., and Delfanian, F., 2013, "Applying an Energy-Based Fatigue Life Prediction Method to Unnotched and Notched Al6061-T6 Specimen," International Mechanical Engineering Congress and Exposition, ASME, San Diego, California.

[6] Scott-Emuakpor, O., George, T., Cross, C., and Shen, M.-H. H., 2010, "Hysteresis-loop representation for strain energy calculation and fatigue assessment," J. Strain Anal. Eng. Des., **45**(4), pp. 275–282.

[7] Scott-Emuakpor, O. E., Shen, H., George, T., and Cross, C., 2008, "An Energy-Based Uniaxial Fatigue Life Prediction Method for Commonly Used Gas Turbine Engine Materials," J. Eng. Gas Turbines Power, **130**(6), pp. 1–15.

[8] Scott-Emuakpor, O., George, T., Cross, C., and Shen, M.-H. H., 2012, "Multi-Axial Fatigue-Life Prediction via a Strain-Energy Method," AIAA J.

[9] Jahed, H., Varvanifarahani, A., Noban, M., and Khalaji, I., 2007, "An energy-based fatigue life assessment model for various metallic materials under proportional and non-proportional loading conditions," Int. J. Fatigue, **29**(4), pp. 647–655.

[10] Letcher, T., Scott-Emuakpor, O., George, T., and Holycross Casey, 2013, "geometric sensitivity ANALYSIS and improved empirical observation FOR REDUCED-ORDER FATIGUE LIFE ASSESSMENT," MFPT and ISA's 59th international instrumentation symposium, Cleveland, Ohio.

[11] Fatemi, A., 2004, "Fatigue behavior and life predictions of notched specimens made of QT and forged microalloyed steels," Int. J. Fatigue, **26**(6), pp. 663–672.

[12] Sherafatnia, K., Kahrobaiyan, M. H., and Farrahi, G. H., 2014, "Size-dependent energy release rate formulation of notched beams based on a modified couple stress theory," Eng. Fract. Mech., **116**, pp. 80–91.

[13] Carlyle, J. M., and Scott, W. R., 1976, "Acoustic-emission fatigue analyzer," Exp. Mech., **16**(10), pp. 369–372.

[14] Roberts, T. M., and Talebzadeh, M., 2003, "Acoustic emission monitoring of fatigue crack propagation," J. Constr. Steel Res., **59**(6), pp. 695–712.

[15] Kohn, D. H., Ducheyne, P., and Awerbuch, J., 1992, "Acoustic emission during fatigue of Ti-6Al-4V: Incipient fatigue crack detection limits and generalized data analysis methodology," J. Mater. Sci., **27**(12), pp. 3133–3142.

[16] Barsoum, F. F., Suleman, J., Korcak, A., and Hill, E. V. K., 2009, "Acoustic Emission Monitoring and Fatigue Life Prediction in Axially Loaded Notched Steel Specimens," J. Acoust. Emiss., **27**, pp. 40–63.

[17] Schumacher, T., Straub, D., and Higgins, C., 2012, "Toward a probabilistic acoustic emission source location algorithm: A Bayesian approach," J. Sound Vib., **331**(19), pp. 4233–4245.

[18] Graff, K. F., 1975, Wave Motion in Elastic Solids, Courier Dover Publications.

[19] "AE Signal Features" [Online]. Available: http://www.ndt-ed.org/EducationResources/CommunityCollege/Other Methods/AE/AE_Signal Features.htm. [Accessed: 14-Jun-2014].

[20] Yu, J., Ziehl, P., Zárate, B., and Caicedo, J., 2011, "Prediction of fatigue crack growth in steel bridge components using acoustic emission," J. Constr. Steel Res., **67**(8), pp. 1254–1260.

[21] Sinclair, A. C. E., Connors, D. C., and Formby, C. L., 1977, "Acoustic emission analysis during fatigue crack growth in steel," Mater. Sci. Eng., **28**(2), pp. 263–273.

[22] Farahmand, B., and Nikbin, K., 2008, "Predicting fracture and fatigue crack growth properties using tensile properties," Eng. Fract. Mech., **75**(8), pp. 2144–2155.

[23] Harris, D. O., and Dunegan, H. L., 1974, "Continuous monitoring of fatigue-crack growth by acoustic-emission techniques," Exp. Mech., **14**(2), pp. 71–81.

[24] Paris, P., and Erdogan, F., 1963, "A Critical Analysis of Crack Propagation Laws," J. Basic Eng., **85**(4), p. 528.

[25] Wertz, J., Shen, M.-H. H., Scott-Emuakpor, O., George, T., and Cross, C., 2011, "An Energy-Based Axial Isothermal-Mechanical Lifing Procedure," Volume 6: Structures and Dynamics, Parts A and B, ASME, pp. 29–36.

[26] “Spearman’s Rank-Order Correlation - A guide to when to use it, what it does and what the assumptions are.” [Online]. Available: https://statistics.laerd.com/statistical-guides/spearmans-rank-order-correlation-statistical-guide.php. [Accessed: 05-Jul-2014].

[27] “ASTM E647 - 08 Standard Test Method for Measurement of Fatigue Crack Growth Rates” [Online]. Available: http://www.astm.org/DATABASE.CART/HISTORICAL/E647-08.htm. [Accessed: 05-Jul-2014].

[28] “ASTM E650 / E650M - 12 Standard Guide for Mounting Piezoelectric Acoustic Emission Sensors” [Online]. Available: http://www.astm.org/Standards/E650.htm. [Accessed: 05-Jul-2014].

[29] “ASTM E976 - 10 Standard Guide for Determining the Reproducibility of Acoustic Emission Sensor Response” [Online]. Available: http://www.astm.org/Standards/E976.htm. [Accessed: 05-Jul-2014].

[30] “Using Median vs. Average” [Online]. Available: http://www.wcc.nrcs.usda.gov/normals/median_average.htm. [Accessed: 05-Jul-2014].